CD No. 114776 المواد المصاحبة
الجامعة الإسلامية - المكتبة - قسم الرسائل الجامعية

Islamic University of Gaza
Deanery of Graduate Studies
Faculty of Science
Physics Department

الجامعة الإسلامية – غزة
عمادة الدراسات العليا
كلية العلوم
قسم الفيزياء

Some Electrical Properties of Doped Poly(9–vinylcarbazole)

By

Wael Abed Ibraheem Tabaza

B. Sc. In Physics Islamic University of Gaza

Gaza

Palestine

537/w t a
1340343
ماجستير

مكتبة الجامعة الإسلامية – غزة
المجموعات الخاصة
التاريخ: 13 -06- 2005
الرقم العام: 1340343
رمز التصنيف: 537/TA
* Electricity

Supervised By

Dr. Taher El-Agez
Associate Prof. of Physics

Dr. Hussian Dawoud
Associate Prof. of Physics
Head of Physics Dept.

Thesis

Submitted to the Faculty of Science as Partial Fulfillment of the Master of Science (M.Sc.) in Physics

2005

بسم الله الرحمن الرحيم

الجامعة الإسلامية - غزة
THE ISLAMIC UNIVERSITY OF GAZA

الرقم: ..... ج س.غ/35/..... Ref

التاريخ: .....2005/03/23..... Date

هاتف داخلي 1150

نتيجة الحكم على أطروحة ماجستير

بناءً على موافقة عمادة الدراسات العليا بالجامعة الإسلامية بغزة على تشكيل لجنة الحكم على أطروحة الباحث/ وائل عبد إبراهيم طبازة لنيل درجة الماجستير في كلية العلوم/ قسم الفيزياء وموضوعها:

(بعض الخواص الكهربية لمادة "Poly "9-vinylcarbazole المطعمة)

وبعد المناقشة العلنية التي تمت اليوم الأثنين 18 صفر 1426هـ الموافق 2005/3/28 الساعة 1.30 ظهراً، اجتمعت لجنة الحكم على الأطروحة والمكونة من:

د. طاهر العاجز	مشرفاً ورئيساً	.....
د. حسين داود	مشرفاً	.....
أ.د. محمد شبات	مناقشاً داخلياً	.....
د. حسن عاشور	مناقشاً خارجياً	.....

وبعد المداولة أوصت اللجنة بمنح الباحث درجة الماجستير في كلية العلوم/ قسم الفيزياء.

واللجنة إذ تمنحه هذه الدرجة فإنها توصيه بتقوى الله ولزوم طاعته وأن يسخر علمه في خدمة دينه ووطنه.

والله ولي التوفيق،،،

عميد الدراسات العليا

أ.د. أحمد يوسف أبو حلبية

الإهداء

أهدي هذا العمل المتواضع إلى روح الشيخ الشهيد الإمام **أحمد ياسين** والشهيد الدكتور **عبد العزيز الرنتيسي** وأرواح شهداء فلسطين جميعًا وأخص منهم أبناء إخوتي الشهيد **عبد الحليم محمد طبازة** والشهيد **إبراهيم جمعة طبازة**، كما وأهدي هذا العمل المتواضع إلى عائلتي و إلى أقاربي و أصدقائي.

ACKNOWLEDGEMENTS

It gives me pleasure to express my thanks to all those who have assisted me in the preparation of this study. My sincere gratitude goes to my supervisor Dr. Taher El-Agez and Dr. Hussian Dawoud, for useful discussions, kind help, and guidance throughout this work.

I would like to express my utmost appreciation and great thanks to Dr. Ahmed Tayyan for his assistance in some discussion and helpful guidance throughout this work.

Special thanks to my colleagues and staff in the Physics Department at the Islamic University of Gaza, for their encouragement and assistance during the time of writing this thesis.

CONTENTS

CONTENTS

LIST OF FIGURES

LIST OF TABLES

ABSTRACT

Several measurements have been performed on films of poly (9–vinylcarbazole) doped with iodine. These measurements include DC conductivity, AC conductivity, and photovoltaic effect.

The DC conductivity of doped films have been studied. The current – electric field dependence was found to obey Schottcky emission mechanism. The experimental value of Schottky coefficient β_{RS} was calculated from the current–electric field dependence. The experimental value of β_{RS} was found to be different from the theoretical value. Its value increased as the thickness of the film was increased.

The thermal activation energy of DC conductivity ε_{ac} was studied for doped samples at various dopant concentrations. The activation energies ε_{ac} for all samples were found to be typical of electronic conduction.

The AC conductivity of doped films was found to increase almost linearly with frequency until $0.5MHz$. Then some kind of saturation was reached. It was found that the AC conductivity does not depend on film thickness and no role was played by the dopant molecule.

Double layer films (ITO- PVK doped with I_2- Rhodamine 6G -Al) were found to exhibit low photovoltaic effect with a curve fitting factor c.f. equal to 0.54, a short circuit current I_{sc} equal to 4.46 nA, and an open circuit voltage V_{oc} equal to 7.7mV.

الملخص العربي

لقد تم في هذه الدراسة اجراء العديد من القياسات لرقائق من مادة Poly(9–vinylcarbazole) المطعمة بمادة الأيودين (I_2)، وقد اشتملت الدراسة على قياس توصيلية التيار المستمر وكذلك توصيلية التيار المتردد وقياس تأثير الجهد الكهروضوئي.

لقد وجد ان توصيلية التيار المستمر لهذه الرقائق تعتمد على المجال الكهربي وأن آلية التوصيل الكهربي في هذه العينات من خلال تحليل النتائج هي آلية Schottky emission mechanism وقد تم حساب القيم التجريبية للمعامل β وقد وجدت أن هذه القيم التجريبية تختلف عن القيم النظرية لها ولكنها في نفس المجال (the same order).

ولقد احتوت الدراسة على قياس طاقة التنشيط Activation Energy لتوصيلية التيار المستمر ووجد ان طاقة التنشيط خاصة بالتوصيل الكتروني .

لقد اشتملت هذه الدراسة على دراسةعينات تحتوي على طبقتين حيث أضيفت طبقة أخرى من مادة Rhodamine 6G بالتبخير فوق طبقة Poly(9–vinylcarbazole) وقيست آلية التوصيل فوجدت أنها أيضاً Schottky emission mechanism ، وعندما تم تعريضها للضوء ظهر تأثير الجهد الكهروضوئي photovoltaic effect ومن خلال النتائج تم حساب curve factor ، ووجد أن قيمته تساوي 0.54 .

CHAPTER I

INTRODUCTION

Introduction

1.1 Fundamental Aspects of Polymer Molecules

The term "polymer" comes from the Greek words poly (meaning "many") and mer (meaning "units" or " parts "). Polymers are very large organic molecules formed by thousands of repeating units linked together. One can view these heavy organic molecules (molecular weights ranging from about 10^3 to 10^7) as very long chains mostly made of C-C, C-O and C-N bonds. Polymer technology has existed for decades and is used for the synthesis of natural rubber and common plastics such as polythene which dates back to as early as 1820s [1,2].

The simplest organic polymer is polyethylene. Consider the single chemical unit shown in fig. 1.1. This unit is called ethylene (or ethene), which consists of two carbon atoms and four hydrogen atoms. A double covalent bond exists between the carbon (C) atoms while a single covalent bond exists between the hydrogen (H) and carbon atoms. The chemical composition of the ethylene mer is written as $C_2 H_4$ or $CH_2 = CH_2$. Under the proper conditions, one of the double covalent bonds between the two carbon atoms can be broken, which enables each of the carbon atoms to form a new covalent bond with a carbon atom in a neighboring mer. In this way three ethylene mers form a "new" molecule, whose atomic weight is three times as great as the initial mer. If "n" ethylene mers join together, the chemical composition of the resulting molecule can be represented as $C_{2n}H_{4n}$, where n is any positive integer. In this way a "chain" of ethylene mers join together to form the well- known polymer

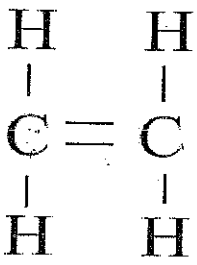

Figure 1.1 The monomer "ethylene".

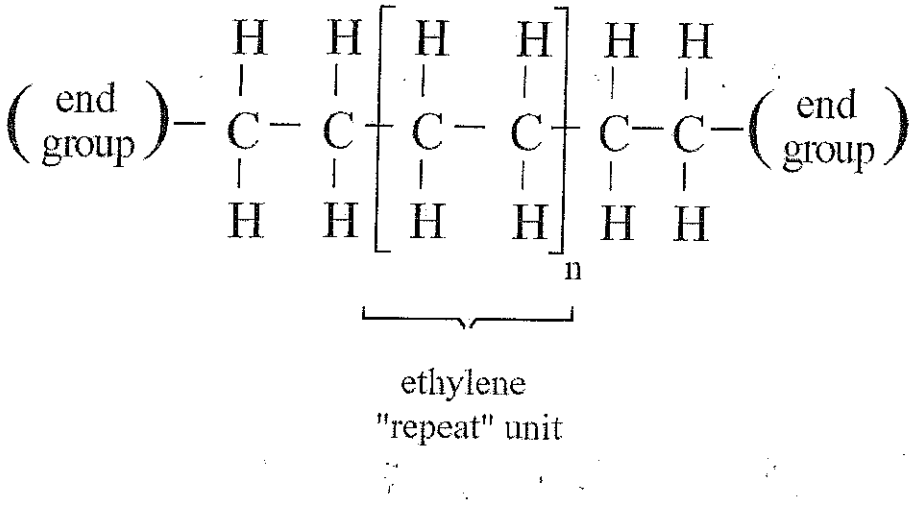

Figure 1.2. Schematic representation of polyethylene. The "mer" and chain structure of carbon and hydrogen atoms are shown.

polyethylene, as shown in fig. 1.2. A typical polyethylene molecule may contain 50,000 carbon atoms or more.

A single ethylene unit is called a monomer, and if two ethylene monomers bond together the resulting chemical entity has two repeating units and is called a "dimer". Similarly, the chemical entity formed by three repeating units is called a "trimer". The molecular weight of a dimer is twice that of the monomer, the molecular weight of a trimer is three times that of the monomer, and so on [2,3,4].

The process of causing a monomer to chemically react and form long molecules in this fashion is called polymerization, and the number of repeating units in the polymer molecule is called the degree of polymerization (DP) [2,5]. The product of the molecular mass of monomer M_m and the degree of polymerization n equals the molecular weight of the polymer M_{pol} [3]:

$$M_{pol} = nM_m$$

Polymers with a high degree of polymerization (molecular weights ranging from about 10^4 to 10^6) are called high polymers, while those with a low degree of polymerization (molecular weights ranging from about 500 to 6000) are known as oligomers [3].

A macromolecule may consist of monomers of identical or of different chemical structure. If only one type of monomer is employed to form a polymer, the resulting molecule is called homopolymer. Polyethylene is a good example of a homopolymer. Polymeric compounds that consist of two or more

types of constitutional repeating units are called mixed polymers or copolymers. Acrylonitrile-butadiene-styrene is an example of a common copolymer, known as "ABS" [3,4,5].

1.2 Types of Polymer Molecular Structure

1.2.1 Homopolymers

The molecular structure of homopolymers can be classified according to one of three major types: linear, branched, and crosslinked (three-dimensional) structure. The three types of molecular structure are shown schematically in fig. 1.3 (denoting a monomeric residue by A and B) [2,3,5].

Linear Polymers

In a bulk sample of linear polymer those long macromolecules become entangled and twisted together, much like as beads on a string, where each bead represents a monomer unit. It should be emphasized that the length of these "strings" is enormous; if a typical linear molecule were scaled up to be 10 mm in diameter, it would be roughly 4 km long. A linear polymer is formed by difunctional monomer. Obviously, as the molecular weight (i.e., the length) of the polymer molecule increases, the number of entanglements increases, and the secondary bonding forces between molecules increase [2].

Branched Polymers

In branched polymers, a relatively short side chains are attached to the main chain (primary backbone) of the macromolecule (see Fig. 1.3.b). The monomers that form branched polymers must be at least trifunctional [2,3,5].

Crosslinked or Network Polymer

The monomers that form crosslinked polymers must be at least trifunctional. Crosslinked polymers consist of long chains connected up into a three-dimensional network by chemical crosslinks. Since the individual molecular chains within a crosslinked polymer are themselves linked together by covalent bonds, the entire molecular network can be considered as a single molecule. Common examples of a crosslinked polymer are natural rubber, silicon rubber, and epoxy.

1.2.2 Copolymers

Copolymers may also be classified according to the arrangement of the monomer units in the macromolecules. The simplest type of copolymers contains only two types of monomer units A and B. Copolymer may be linear or branched (see Fig. 1.4) [2,4,5]. In linear random copolymers, the two distinct repeating units appear randomly along the backbone of the molecule. In contrast, for linear block copolymers, each type of repeat units form fairly long continuous sequences within the polymer chain [2,3]. In branched copolymers a short side chains repeat units B are attached to the primary backbone with repeat unit A of the macromolecule, such materials are called graft copolymers.

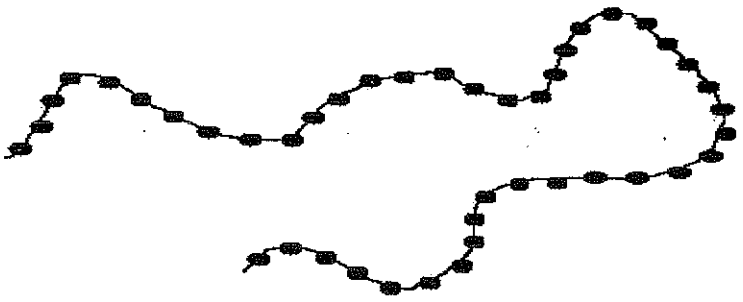

(a)

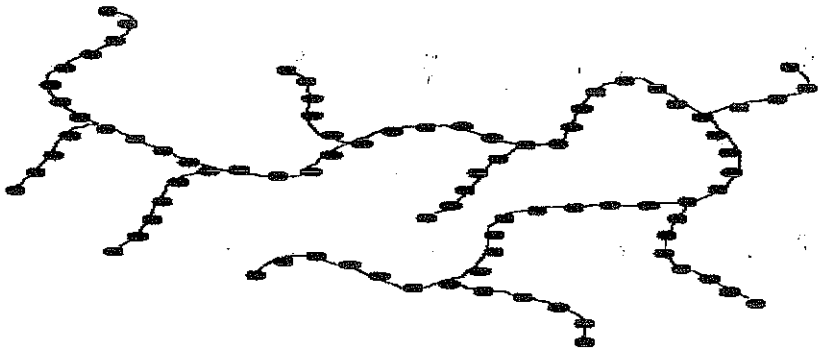

(b)

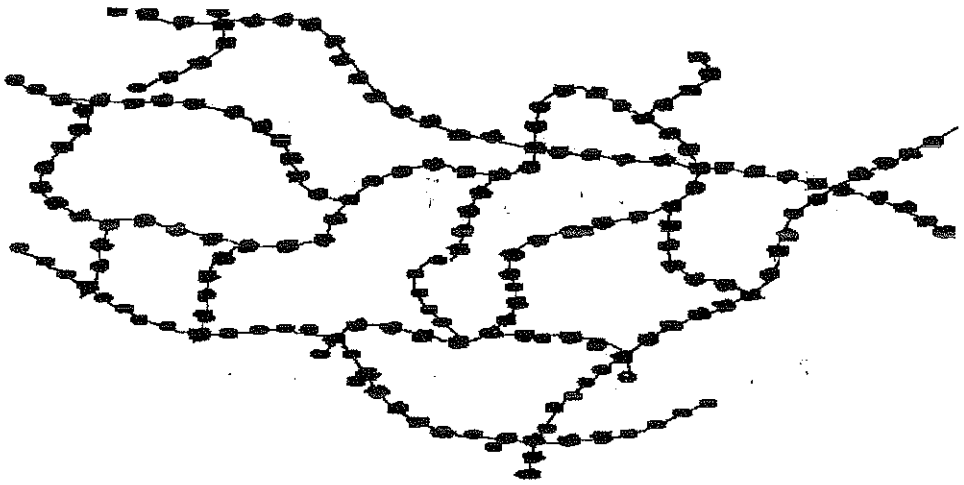

(c)

Figure 1.3. The three types of molecular structure (a) Linear polymer, (b) Branched polymer and (c) Crosslinked or network polymer.

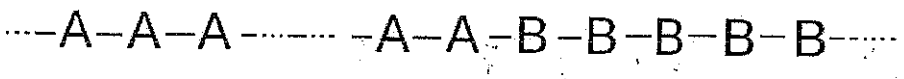

(a)

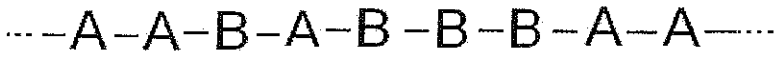

(b)

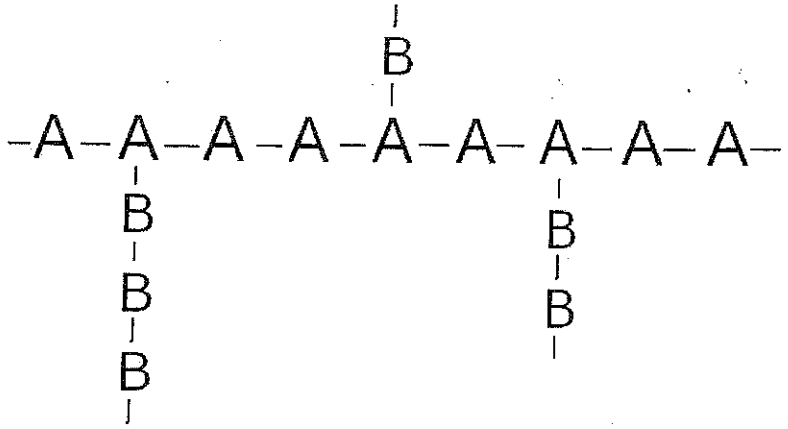

(c)

Figure 1.4. Types of Copolymers, (a) Linear block copolymer, (b) Linear random copolymer and (c) Graft copolymer.

1.3 Polymerization Processes

The process that converts a monomer to a polymer is called polymerization. There are two different methods of polymerization processes, polycondensation and addition polymerization [5,6]. During the formation of a polymer the condensation takes place between two polyfunctional molecules, with the possibility of elimination (migration) of some molecules such as water, and the reaction continues until one of the reagents is used up [3,5].

Addition or chain reaction polymerization consists of activation or initiation of the monomer molecule converting an ion to a free radical. The free radical reacts with the double bond of an unexcited monomer molecule and adds to it, forming a new radical capable of further interaction with the initial monomers. In a short period of time more monomers add successively to the growing chain. At last, two free radicals annihilate each other's growth activity forming one or more polymer molecules [3,7].

1.4 Classification of Polymers

Polymers are classified according to their chemical composition into three main categories [3, 5]:

1- Organic polymers include polymeric substances containing other elements in their molecules provided that the main chain are not connected directly to carbon atoms (e.g., organic polyacid salts).

2- Elemento-organic (or hetero-organic) polymers include:

(a) compounds whose chains are composed of carbon atoms and hetero-atoms (except for nitrogen, sulphur, and oxygen atoms).

(b) compounds with inorganic chains if they contain side groups with carbon atoms connected directly to the chain.

(c) compounds whose main chains consist of carbon atoms and whose side groups contain hetero-atoms (except for nitrogen, sulphur, oxygen, and halogen atoms) connected directly to the carbon atoms of the chain.

3- Inorganic polymers are polymers containing no carbon atoms.

1.5 Thermoplastic and Thermoset Polymers

Suppose that a bulk sample of a linear or branched polymer exists as a solid material at room temperature, and is subsequently heated, then the average distance between individual molecular chains is increased as temperature is increased. Subsequently, this results in an increase in the molecular mobility and a decrease in the secondary bonding forces and the macroscopic stiffness. That is, as the molecules move apart both the intermolecular forces of attraction as well as the degree of entanglement is decreased, resulting in a decrease in stiffness at the macroscopic level. Eventually, a temperature is reached at which the polymer starts to melt where the polymeric molecules can slide freely past each other and the polymer can no longer support a shear force.

A polymer that can be melted (i.e., a linear or branched polymer) is called a thermoplastic polymer [2]. Examples of thermoplastic polymers include polyethylene, PVC, polystyrene, polypropylene, acrylics, nylons, polycarbonates, polyesters, and fluoroplastics [8]. Thermoplastics can be sub-divided into those which crystallize on cooling and those which do not

crystallize on cooling. The ability of polymers to crystallize depends upon many factors such as the degree of branching and the regularity of molecules [4]. In contrast, a crosslinked polymer cannot be melted, although the average distance between individual segments of the molecular network are in fact increased as temperature is increased. The crosslinks do not allow unrestricted relative motion between chain segments, and eventually limit the molecular motion. Therefore, a crosslinked polymer cannot be melted and can support shear forces even at high temperatures. Of course, if the temperature is raised high enough the covalent bonds that form the crosslinks as well as the backbone of the molecular chains are broken, chemical degradation occurs, and the polymer is destroyed. A polymer that cannot be melted is called a thermoset polymer. Examples of thermosetting polymers include epoxies, silicones, polyesters, amino resins, and polyurethane [2,9].

1.6 The Glass Transition Temperature

The temperature affects the macroscopic stiffness of both thermoplastic and thermoset polymers. All polymers exhibit a decrease in stiffness near a characteristic temperature called the glass-transition temperature T_g. It is the temperature at which the polymer is transformed from a relatively "glassy" and brittle solid to a relatively "rubbery" and ductile solid. This transition is due to an increase in the mobility of large segments of the main polymeric chain. That is, when a polymer has been heated to the T_g the associated increase in the average molecular spacing results in a sharp decrease in the secondary bonding

forces, allowing segments of the polymer molecules to each "slide" past each other [2,10].

At temperatures significantly below T_g the polymer molecules are closely packed and tightly bonded by secondary bonding forces, and cannot easily slide past each other. The polymer is said to be in a "glassy" state at lower temperatures, and exhibits a high stiffness and strength but in general a lower ductility. Conversely, at a temperatures significantly above the T_g the molecular spacing is increased and hence secondary forces are greatly decreased such that large segments of molecular chains can more readily slide past each other. The polymer is said to be in a "rubbery" state at these higher temperatures, and exhibits a lower stiffness and strength but in general higher ductility. The preceding discussion of transition temperatures has been based on observed changes in stiffness. However, almost any physical property measured at the macroscopic level will exhibit a similar dependence on temperature. Thus, the T_g can be measured by monitoring polymers stiffness, density, and thermal expansion [2,10].

1.7 Poly(N-vinylcarbazole)

Graebe and Glaser discovered Carbazole (dibenzopyrrole) in 1872 as a by-product from the coal tar industry. Pure Carbazole is a white crystalline material with a melting point of 246°C and a molecular weight of 167.20 g/mole. Carbazole, an aromatic tricyclic compound, exhibits strong fluorescence and long phosphorescence upon exposure to ultraviolet light. It is readily soluble in acetone, slightly soluble in ether and ethanol, and barely

soluble in chloroform, acetic acid, carbon tetrachloride, and carbon disulfide [11].

Carbazole is also used to synthesize the monomer N-vinylcarbazole, which can be polymerized to form poly(N-vinylcarbazole). The I. G. Farbenindustrie in Germany began the production of poly(N-vinylcarbazole) (PVK) under trade name Luvican. The shortage of mica during the World War II was the reason for the development of poly (N-vinylcarbazole), under trade name Polectron (General aniline and Film Corp.), as a mica substitute [5, 11].

Poly(N-vinylcarbazole) (PVK) can be polymerized by both free radical and cationic polymerization. The propagating chain end stabilizes electron deficient centers by resonance, involving the nonbonding electron pair on the nitrogen of the Carbazole ring. N-Vinyl Carbazole has not been successfully polymerized by anionic means [11]. The number 9 in Poly(9-vinylcarbazole) indicate that the vinyl group is attached to the nitrogen in the Carbazole molecule. The structure formulas of poly(9-vinylcarbazole) is shown in fig. 1.5. We can categorize poly (9-vinylcarbazole) as an organic homopolymers since it consists of only one type of constitutional repeating units, also, it is a heterochain polymer since its main chain made up of different kind of atoms [5].

1.8 Properties of Poly(9-vinylcarbazole)

Poly(9-vinylcarbazole) is a transparent thermoplastic material, with a good thermal and chemical stability. For example, it has a softening temperature of 150°C, a reported glass transition temperature T_g of 211°C, and

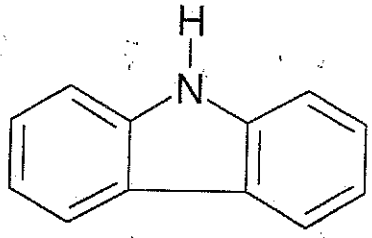

(a)

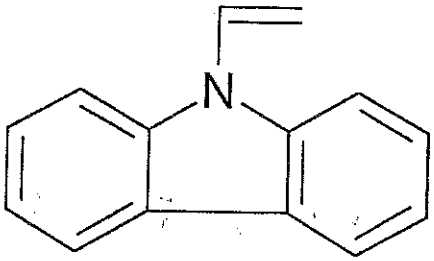

(b)

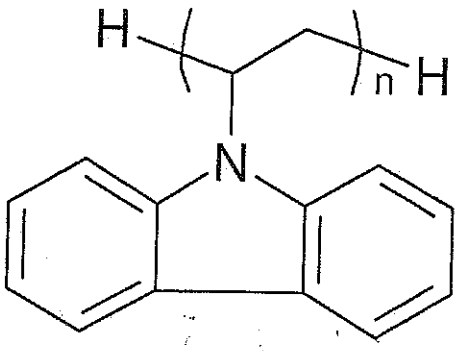

(c)

Figure 1.5 The structure formulas of poly(N-vinylcarbazole), (a) Carbazole, (b) N-vinylcarbazole, and (c) Poly(N-vinylcarbazole).

does not begin to decompose until over 300°C. The glass transition temperature of this polymer is high. Unfortunately, poly(9-vinylcarbazole) is brittle and has a poor mechanical strength. Poly(9-vinylcarbazole) has a high refractive index of 1.69 at 20°C. The solvents of Poly(9-vinylcarbazole) are aromatic hydrocarbons, chloroform, chlorobenzene, methylene chloride, and tetrahydrofuran (THF) [12]. Poly(9-vinylcarbazole) is also a photoconductive material: it behaves like an insulator in the dark, and becomes electrically conductive upon exposure to ultraviolet radiation. Since a practical usage employs visible light, the photosensitivity of the polymer must be extended into the visible. There is an enormous literature dealing with the subject of sensitization, and yet despite this, major questions remain unanswered about the details of this technologically and scientifically important phenomenon. With intense laser light, Poly(9-vinylcarbazole) can undergo a change in refractive index and thus is considered a photorefractive material. Poly(9-vinylcarbazole) also has other excellent electronic properties, such as low dielectric loss [11].

Poly(9-vinylcarbazole) has been the subject of considerable research due to its application as photoreceptors in photocopying technology. Recently, interest has developed in photoconducting material applications in electroluminescent, photorefractive, photovoltaic, and transistor devices [13, 14, 15].

1.9 Methods of Polymer Doping

In inorganic semiconductors doping occurs via the introduction of dopant atoms that provide additional free charge carriers at room temperature so that the extra charges increase the conductivity for this type of semiconductor. The electrical conductivity of polymers is markedly increased upon doping. Thus, various methods for doping of polymers have been employed. Among these methods are [16, 17]:

a. Doping with Gaseous Vapors

This method is applied for doping of the organic polymer by vapor substances (e.g., I_2, SbF_5, Br_2, and AsF_5), and may be achieved by the exposure to vapors of the dopants.

b. Photo-Initiated Doping

When organic polymer is exposed to radiation of energy greater than its band-gap, electrons are promoted across the gap and the polymer undergoes 'photo-doping'. It disappears rapidly due to recombination of electrons and holes when irradiation is discontinued. If a potential is applied during irradiation, then the electrons and holes separate and photoconductivity is observed.

c. Solution Doping

This method is used when the polymer is soluble in the organic solution e.g., tetrahydrofuran THF, chloroform. The outcome of such doping method is an n- type doped polymer

d. Doping by Oxidizing Cations

This method can be carried out by using salts that contain NO_2^+ or NO^+ ions to produce p- type doping material. The salts oxidize the organic polymer and introduce anions in the lattice.

e. Chemical or Electrochemical Doping

The p-doping can be accomplished by electrochemical anodic oxidation by immersing, for example, a trans-$(CH)_x$ film in a solution of $LiClO_4$ dissolved in propylene carbonate and attaching it to the positive terminal of a dc power source, the negative terminal attached to an electrode is also immersed in the solution.

The n-doping can also be carried out by electrochemical cathodic reduction by immersing a trans-$(CH)_x$ film in, e.g. a solution of $LiClO_4$ dissolved in THF and attaching it to the negative terminal of a dc power source, the positive terminal attached to an electrode is also immersed in the solution.

1.10 The Aim of This Work

We study poly(9–vinylcarbazole) doped with various types of dopants in order to improve its electrical conductivity. Our goal has been to develop a type of doped polymer that can be used for electronic applications. Some reports [18,19,20] show that the electrical conduction mechanism in this doped polymer is not yet quiet well understood, and more theoretical and experimental work are required to understand its nature.

It seems that most research, so far, conducted on Poly(9–vinylcarbazole) has focused on various photoconductivity measurements. While measurements

on Dc electrical conductivity of doped Poly(9–vinylcarbazole) are very rare. We believe that doped Poly(9–vinylcarbazole) is a promising material. It may offer good opportunities to researchers to investigate. Much work is needed to be done on this material in order to bring insight on various electrical conduction properties such as transport, conduction mechanism, trapping, the role of dopant molecules, etc. .

In this thesis we report our work on doped Poly(9–vinylcarbazole) which we have extensively studied.

CHAPTER II

BACKGROUND ON POLYMER ELECTRICAL CONDUCTIVITY

Background on Polymer Electrical Conductivity

2.1 Introduction

Electrical conductivity in a normally insulating polymer is made possible by doping. It is universally agreed that the conductivity in doped polymers is a direct consequence of the proportionate amount of dopant in the sample being tested. [21]. The conductivity changes with the range of the doping level and the type of the dopant. Shirakawa achieved conductivity on the order of 10^3 S/cm for polyacetylene doped with iodine, [22]. In 1987 Naarmann et al produced conductivity on the order of 10^4 S/cm [23], and in 1990 Tshukomoto had increased it to 10^5 S/cm [24]. Although initially these doped conducting polymers were unstable in air and difficult to process, new generations of conducting polymers are greatly improved to be air-stable and easily processable from a variety of solvents [25].

It is known that the electrical conductivity depends on the size of the bandgap between the valence band and the conduction band. For insulators, the band-gap is typically several times larger than the semiconductor band-gap. On the other hand, for semi-conductor the energy gap is small, e.g. 1 eV, and the electrons can easily be excited into the conduction band by several means such as thermal excitation, vibrational excitation and photoexcitation. Most semiconducting polymers appear to have a band-gap that lies in the range 1.5–3 eV, which makes them ideally suite as optoelectronic devices working in the visible light range [26].

Poly(phenylenevinylene) (PPV), with a band-gap of 2.2 eV can be considered as an example of an intrinsic polymeric semiconductor [1]. For a conduction to take place in conventional inorganic semiconductors, like silicon or germanium, free electrons must generally be excited from the valence to the conduction band. Normally, photo excitation or thermal excitation at room temperature gives rise to some conductivity in many inorganic semiconductors.

Unlike the widespread inorganic compounds, doped polymers are semiconductors as a result of their unique, extended π-conjugation. Indeed the extended-overlap π-bands become the valence band and the π* bands become the conduction band in conducting polymers (CPs). The π-conjugated system is formed by the overlap of carbon p_Z orbitals. The chemical bonding between the atoms in the main carbon ''backbone'' of the polymer chain alternates between single and double bond lengths which is the common electronic feature of pristine (undoped) conducting polymers. The semiconducting behavior of polymers originates from those delocalized π-orbitals formed in carbon-containing compounds [1,26,27]. The pristine electronic polymers can be transformed to their conducting form by simple chemical or electrochemical oxidation, or in some cases, reduction, by a number of simple anionic or cationic species (dopants) [27].

Conjugated polymers can be easily oxidized or reduced, and when oxidized, electrons are removed from conjugated polymers and counter ions (anions) are introduced into the system such that the local charge neutrality is

preserved, causing *p*-doping (electron accepting-e.g., I_2, PF_6, Cl, and AsF_6). On the other hand, when reduced, electrons are added to the polymer chains. Counter ions (cations) are also introduced to the polymer system to preserve the charge neutrality, yielding n-doping (electron donating-e.g. Na, K, Li, Ca, and tetrabutylammonium) [20]. In short, p-*type* doping is electron accepting and n-*type* is electron donating. Compared to the intrinsic semiconducting polymers, the conductivity of doped conjugated polymers increases by several orders of magnitude and approaches that of metallic conductors in some cases [1]. Since conjugated polymers can be easily processed into thin films they can be used as the active material in a number of applications, including photovoltaic, light emitting diodes (LEDs), rechargeable batteries, sensors, corrosion protection, electro-optics, electromagnetic interference shielding, microwave-based technologies, electrochromic devices, and field effect transistors (FETs) [28,29]. Furthermore, the polymers are lightweight and flexible, with many of their properties being adjustable to suit specific requirements.

2.2 Models that Discuss Electrical Conductivity in Insulating Film

The current across a metal-semiconductor junction is mainly due to the motion of majority carriers. Different mechanisms that explain the flow of carriers from a semiconductor to a metal were introduced. Among these mechanisms are:

2.2.1 Schottky Emission

Schottky effect is the increase in the discharge of electrons from the surface of a heated material by application of an electric field that reduces the value of the energy required for electron emission. The heat supplies the minimum energy required for an electron to escape the surface of a specific material, called the work function ϕ. A very weak electric field may be applied that simply sweeps the already emitted electrons away from the surface of the material. When the field is increased, a point is reached for quite moderate fields at which the value of the work function itself is lowered. As the applied field (voltage) is further increased, the work function continues to decrease, so that the electron emission current continues to increase. At very high values of the applied field, however, the electron emission undergoes an excessive increase because of the onset of a different type of emission, called high-field emission or, simply-field emission [30,31].

A Schottky barrier is created by contact of a metal and a semiconductor surface. Fig. 2.1 shows the situation of a Schottky barrier at a metal and a p-type semiconductor junction. The Fermi levels of a metal and a semiconductor before

contact is shown in fig. 2.1.a. This difference in Fermi levels will cause electrons to flow from the semiconductor to the metal when brought together where a region of uncompensated charged acceptors results. This "space charge" causes a voltage drop at the interface[32]. When an electric field is applied across the junction the electric current density is given by the following expression [31]:

$$J_S = RT^2 \exp\left(-\frac{e\phi_{RS}}{kT}\right)\exp\left(\frac{e}{kT}\sqrt{eE/4\pi\varepsilon_s}\right) \qquad (2.1)$$

Where R is Richardson's constant, T is the absolute temperature, ϕ_{RS} is the electrode dielectric work function, ε_s is the dielectic constant, k is Boltzman's constant, E is the applied electric field, and e represents the electronic charge. Equation 2.1 can be written as:

$$\ln I_{RS} = const + \frac{e\beta_{RS}}{kT}E^{1/2} \qquad (2.2)$$

Where β_{RS} is the Schottky coeficient given by

$$\beta_{RS} = \left(\frac{e}{4\pi\varepsilon_s}\right)^{1/2} \qquad (2.3)$$

Equation 2.2 illustrates a linear relation between $\ln I_{RS}$ and $E^{1/2}$ with slope $\frac{e\beta_{RS}}{kT}$.

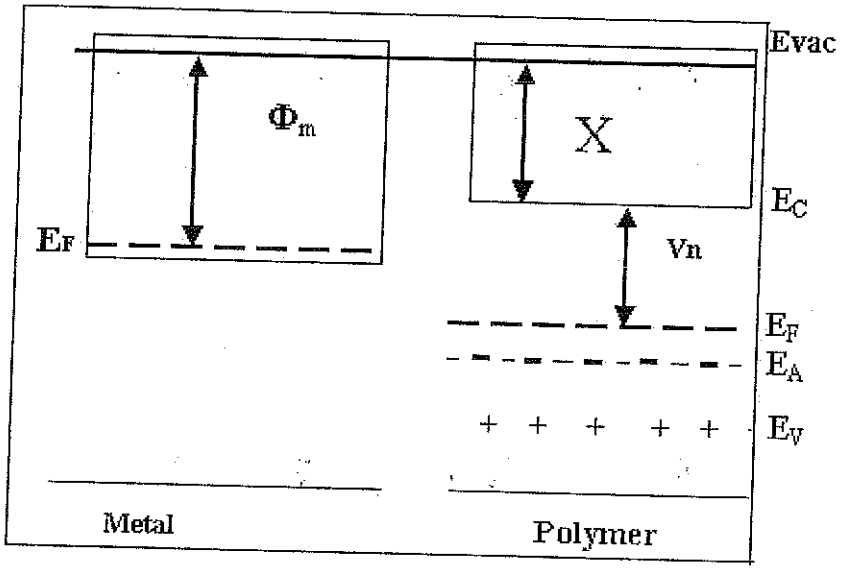

(a)

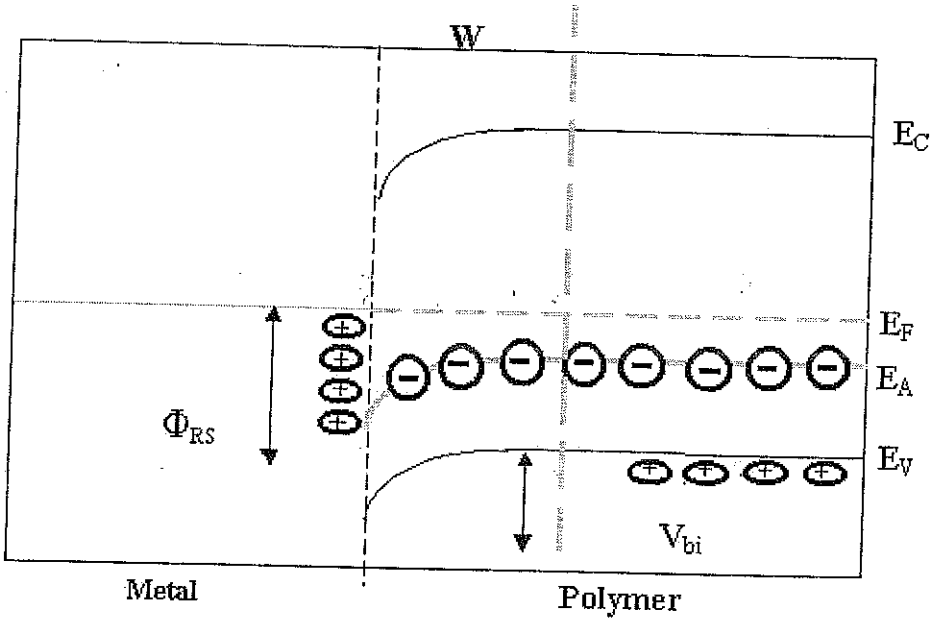

(b)

Figure 2.1. (a) A metal and a semiconductor before contact, and (b) Schottky barrier formed after contact of the metal and the semiconductor. Where V_{bi} is the built-in voltage, W is depletion width, Φ_{RS} is the barrier height, and Φ_m is the work function of the metal

2.2.2 **Ohmic Contact**

A metal-semiconductor junction results in an ohmic contact (i.e. a contact with voltage independent resistance) if the Schottky barrier is zero or negative. In such case, the carriers are free to flow in or out of the semiconductor so that there is a minimal resistance across the contact. For an n-type semiconductor, this means that the workfunction of the metal must be close to or smaller than the electron affinity of the semiconductor. For a p-type semiconductor, it requires that the workfunction of the metal must be close to or larger than the sum of the electron affinity and the bandgap energy. Since the workfunction of most metals is less than 5 eV and a typical electron affinity is about 4 eV, it can be problematic to find a metal that provides an ohmic contact to wide bandgap semiconductors.

2.2.3 **Tunneling**

Tunneling through a barrier of finite width becomes possible with the presence of an electric field across a junction. Tunneling is a quantum mechanical effect, such contacts do have a positive barrier at the metal-semiconductor interface, but also have a high enough doping in the semiconductor that there is only a thin potential barrier separating the metal from the semiconductor. If the width of the depletion region at the metal-semiconductor interface is very thin then, the wavefunction of an electron in the metal electrode extends into the semiconductor; thus there is some probability that the electron can exist there. Tunneling from a Dirac well with height ΔE into a continuous energy band has

been calculated by a Green's function approach and in Oppenheimer approximation [31, 33]. The current density due to tunneling formula is given by

$$J_T = \frac{e^2 E^2}{8\pi h \phi_b} \exp\left(-\frac{8\pi\sqrt{2m_e}}{3heE} (e\phi_b)^{3/2} \right) \tag{2.4}$$

Where h is Planck's constant, ϕ_b is the electrode work function, and m_e is the electronic mass.

2.2.4 Ionic Conduction

Conduction under high temperature in thick-films and bulk insulators occurs by ionic conduction rather than electronic conduction. Ions are large and heavy carriers of low mobility, also they need high activation energy to execute nearest neighbor diffusive jumps, which causes charge transport. Ionic conduction mechanism is given by the following formula [5]

$$J_T = \frac{aE}{kT} \exp\left(-\frac{\varepsilon_a}{kT} \right) \tag{2.5}$$

Where a is a constant and ε_a is the activation energy.

2.2.5 Intrinsic Conduction

This mechanism is generated from the direct electronic exitation from the valence band to the conduction band. The intrinsic conduction is negligible at low temperature because the energy gap ε_g of the insulator is large. The formula of intrinsic conduction mechanism is given by[5]:

$$J_T = BT^{3/2} \exp\left(-\frac{\varepsilon_g}{2kT}\right)E \tag{2.6}$$

Where B is constant and ε_g is the energy gap.

2.2.6 **Poole-Frankel Emission**

The Poole-Frenkel effect is a classical effect, where the carrier is still emitted by thermal activation over the top of a potential barrier, which is lowered by the presence of an electric field. The electric current density in this mechanism is given by the following expression [5, 31]

$$J_{PF} = AE \exp\left(-\frac{e\phi_{PF}}{kT}\right)\exp\left(\frac{e}{kT}\sqrt{eE/\pi\varepsilon_s}\right) \tag{2.7}$$

where A is a constant, $e\phi_{PF}$ is the depth of potential well, e is the electronic charge, and ε_s is the dielectric constant. Equation 2.7 can be written as:

$$\ln I_{PF} = const + \frac{e\beta_{PF}}{kT}E^{1/2} \tag{2.8}$$

where β_{PF} is the Poole-Frenkel coeficient given by

$$\beta_{PF} = \left(\frac{e}{\pi\varepsilon_s}\right)^{1/2} \tag{2.9}$$

Equation 2.8 illustrates a linear relation between $\ln I_{PF}$ and $E^{1/2}$ with slope $\frac{e\beta_{PF}}{kT}$.

CHAPTER III

THE EXPERIMENTAL TECHNIQUES

The Experimental Techniques

3.1 Introduction

In this chapter, we present the experimental techniques used in this work. It includes a description of samples preparation method, DC electrical conductivity measurements, the activation energy measurements, and other measurements.

3.2 Sample Preparation

Two sets of samples were prepared in this work. The films of the first set consist of a single layer doped with various weight concentrations of iodine I_2. Poly(9–vinylcarbazole) with molecular weight equal to 11×10^5 (available from Aldrich chemical company, inc. Milwaukee) was used. Films with different iodine I_2 dopant based on weight concentrations were prepared (1%, 2%, and 4%). Poly(9–vinylcarbazole) and the dopants were weighted using a sensitive electric balance (Strtorius AG Gottingen model BA1105) with a resolution of $10^{-4}gm$. The second set of samples is composed of double layer films, the first layer consists of poly(9–vinylcarbazole) (doped with I_2 or undoped) and the second thin layer of Rhodamine 6G is deposited on PVK layer by vaccum evaporation. Figure 3.1 shows a schematic drawing of these films.

Previouse studies indicated that a charge transfer complex CT between PVK and iodine is formed [15,34,35].

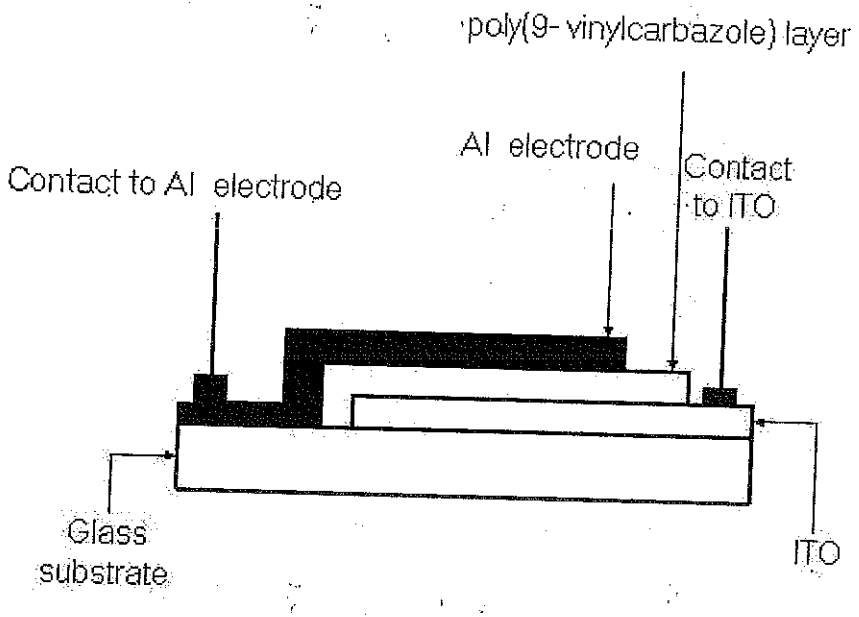

(a)

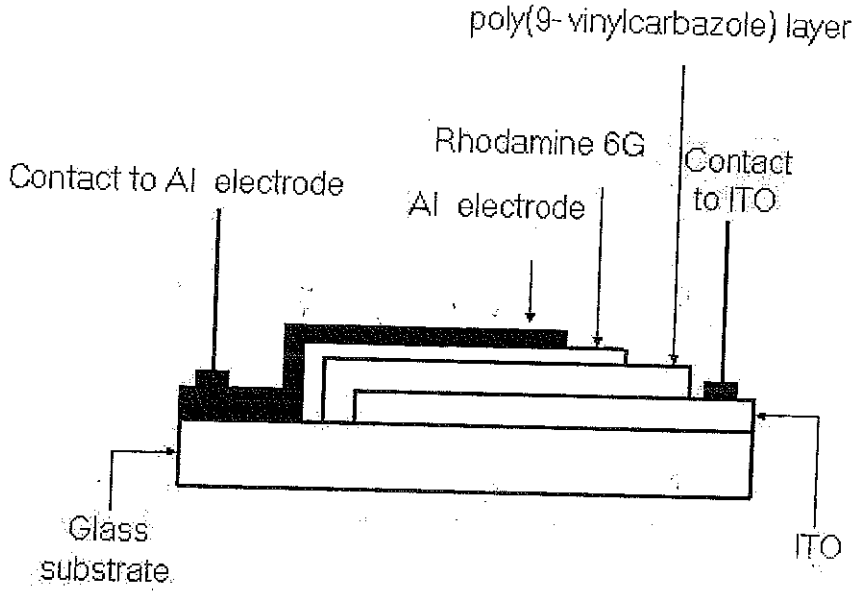

(b)

Figure 3.1. Schematic drawing of (a) a single layer sample, and (b) a double layer sample.

Poly(9–vinylcarbazole) was dissolved in proper a mounts of organic solvents such as chloroform and THF. Then the desired weight concentrations of the dopants iodine I_2 were added to the solution. A homogeneous solution was then obtained by thoroughly stirring this mixture for several minutes. Cleaned electrodes were obtained by thoroughly wiping each electrode surface by a cotton pad wetted with acetone. This procedure was repeated twice for each electrode surface then the electrodes were placed in a beaker containing an organic solvent (chloroform) for twenty minutes. Then the electrodes were oven dried at a temperature of a bout $200C^0$ for one hour. The sample films were then prepared by spin coating few drops of this solution onto the pre cleaned aluminium electrodes or the indium tin oxide (ITO) electrodes. Then, the prepared samples were heated in an oven at $80C^0$ for several hours to remove residual solvent.

The thickness of the films were determined by measuring the capacitance of the samples using a digital LCR meter (Tenma 72-960). The film thickness d was approximately estimated using the following equation

$$d = \frac{\varepsilon_0 \varepsilon_r A}{C}$$

Where ε_0 is the permittivity of free space, ε_r is the relative dielectric constant of poly(9–vinylcarbazole) taken to be equal to 3.0 [5], A is the film area, and C is the capacitance of the sample.

3.3 Experimental Procedure

The sample films in this experiment were arranged in sandwich type configuration i.e. electrode–film–electrode structure. A thin polymer layer of thickness *d* was spin coated between two electrodes of different work functions. The other aluminum electrode was either pressed on the film for the single layer samples or vacuum evaporated for the double layer samples. The DC conductivity measurements of the samples were done in dark, at normal atmosphere, and at room temperature. Also, the variation of the DC conductivity with temperature (at normal atmosphere) was studied. In this case the samples were heated using an electrical heater. The heater was positioned directly beneath the sample. The temperature was measured using a thermocouple of type K(NiCr–NiAl) attached to the sample. This K-type thermocouple was connected to a digital multimeter indicator (model Hc-5010Ec) with a resolution of $1C^0$. The experimental arrangement used in these measurements is depicted in fig 3.2.a.

3.4 Thermal Vacuum Evaporation

The thermal vacuum evaporation deposition technique is established in by heating the material to be deposited in vacuum until evaporation is reached. A scheme of the deposition equipment is illustrated in the fig. 3.3.a. The material vapor condenses in a form of thin film on the cold substrate surface and on the vacuum chamber walls. Usually low pressures are used, about 10^{-5} torr or lower, to avoid reaction between the vapor and atmosphere.

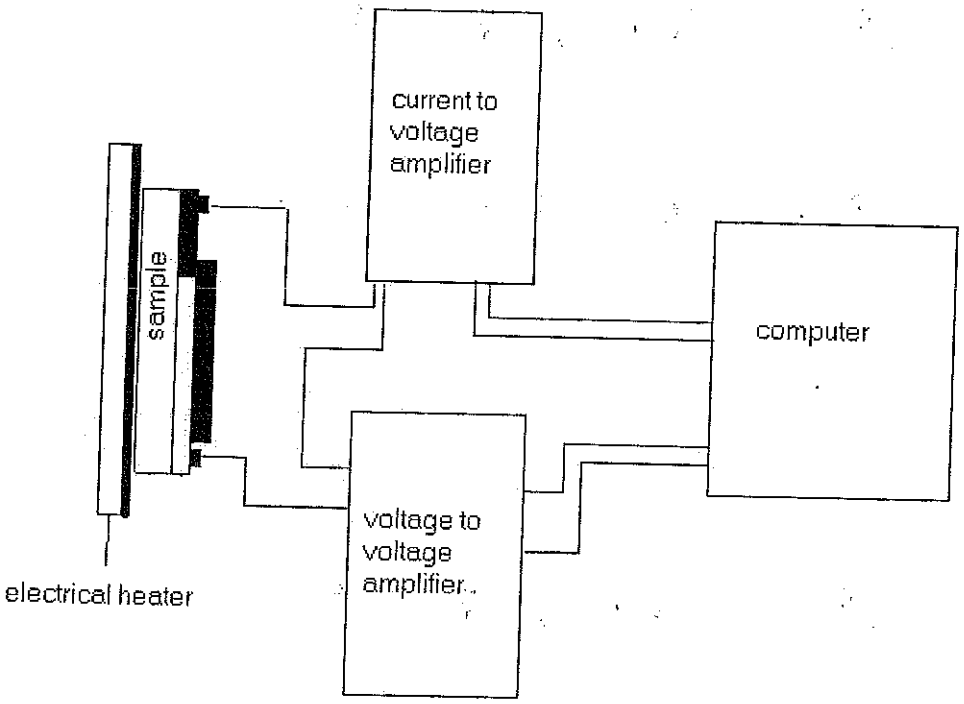

(a)

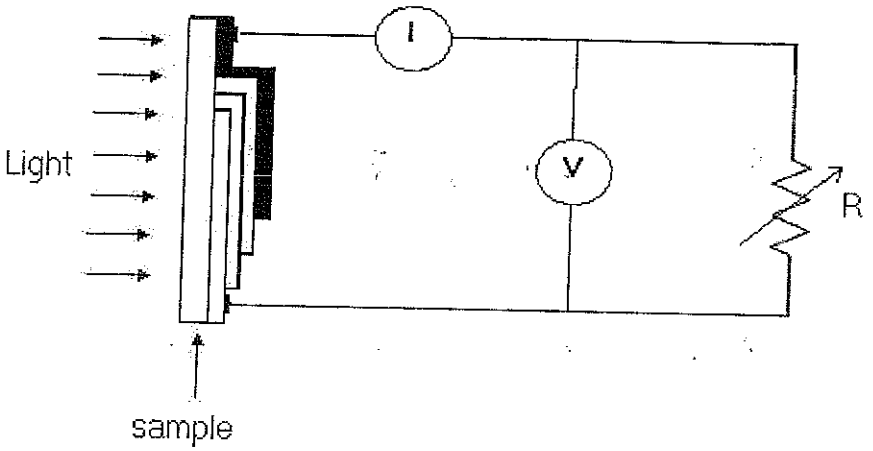

(b)

Figure 3.2. (a) The experimental setup used in measuring the DC conductivity of the single layer samples and (b) the experimental setup used in measuring the photovoltaic effect response of the double layer samples.

At these low pressures, the mean free path of vapor atoms should be of the same order as the vacuum chamber dimensions, so these particles travel in straight lines from the evaporation source towards the substrate. The components of the evaporating system are shown in Fig. 3.3.b. The vacuum is obtained by an Edwards Diffstak 100 water-cooled diffusion pump capable of achieving vacuum pressures in the 10^{-8} torr range at a pumping speed of 280 ls^{-1}. The diffusion pump is equipped with a manual high-vacuum isolation valve and a cooling fail thermal snap-switch, a safety device that will cut the power to the pump heater if the temperature of the cooling water becomes too high. This prevents thermal breakdown of the pump fluid, Santovac 5, into dangerous organic compounds such as benzene or phenolic materials. The Diffstak is backed by an Edwards E2M8 rotary pump that drives up to 14.7cfm of air. The two pumps are connected by a flexible stainless steel pipeline that permits minor position adjustments of the rotary pump.

3.5 Measurement of the DC and the AC Electrical Conductivity

3.5.1 Measurement of the DC Electrical Conductivity

The sample films used in these measurements were arranged in sandwich type configuration that is Al–film–ITO structure. This sandwich configuration was held fixed together by pressing the aluminum electrode to the polymer film (or, by vacuum evaporating the aluminum electrode).

The current – voltage signals were processed through a MetraByte's DAS-20 data aquasition card. MetraByte's DAS-20 is a multifunction, high-

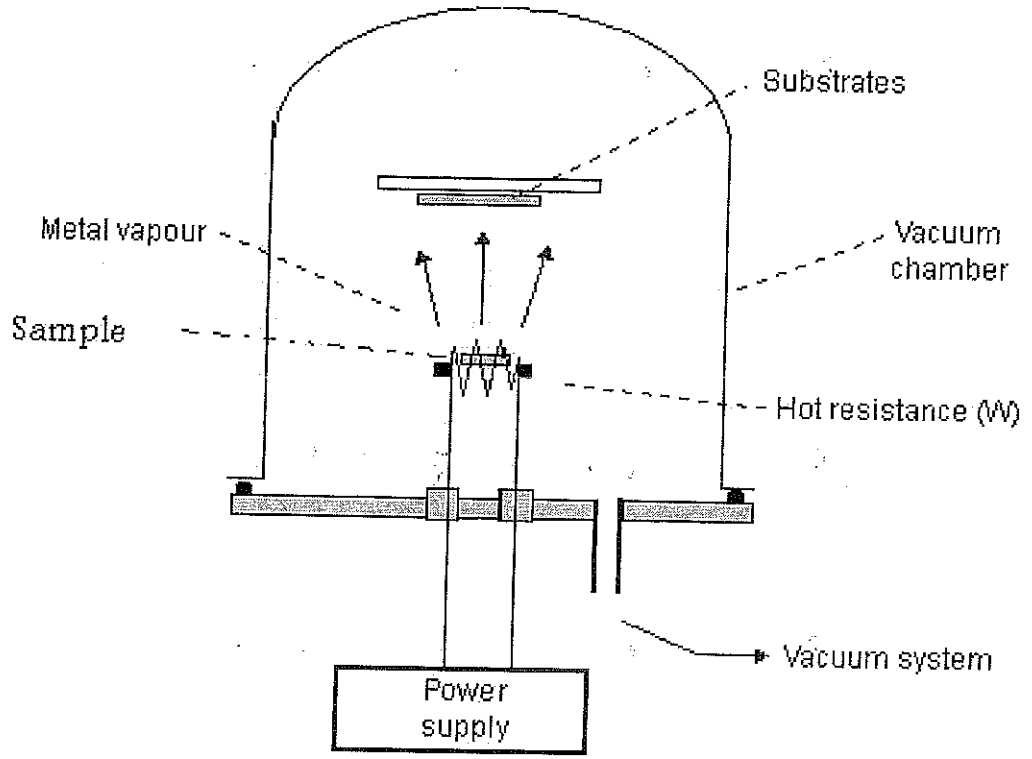

Figure 3.3.a. A schematic setup of the evaporator.

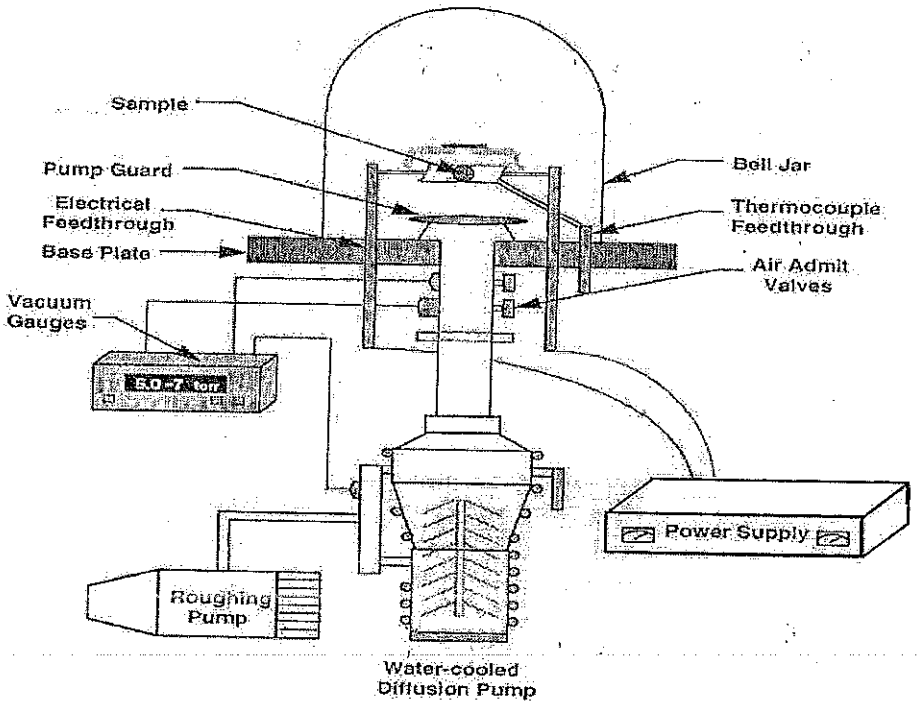

Figure 3.3.b. A schematic of the evaporation experimental apparatus.

speed, A/D (Analog/Digital), I/O expansion board that turns a host computer into a precision data-acquisition and signal-analysis instrument. The board plugs directly into any expansion slot of an IBM PC/XT/ AT, Or PS/2 models 25 and 30, or compatibles. This card has eight analog to digital (ADC) input terminals and two digital to analog (DAC) output terminals. One of these DAC terminals was used to control the voltage across the sample.

Before applying the potential to the sample, the output of this terminal was amplified using a national semiconductor LMI2cl linear amplifier (see fig. 3.4). This combination insured that the input voltage across the sample can be varied from –30 volt to +30 volt. The circuit of the amplifier that has been used in these measurements is shown in fig. 3.4. One of the input terminals was used to measure the voltage across the sample. Another input terminal was used to measure the current passing through the sample via a current to voltage converter fig. 3.5. The output voltage of this amplifier was recorded by the card interfaced to the computer and was converted back into current using the following equation

$$gain = 1 + \frac{R_1}{R_2} + \frac{R_1}{R_F} \qquad (3.1)$$

$$V_{OUT} = gain \times I_{in} \qquad (3.2)$$

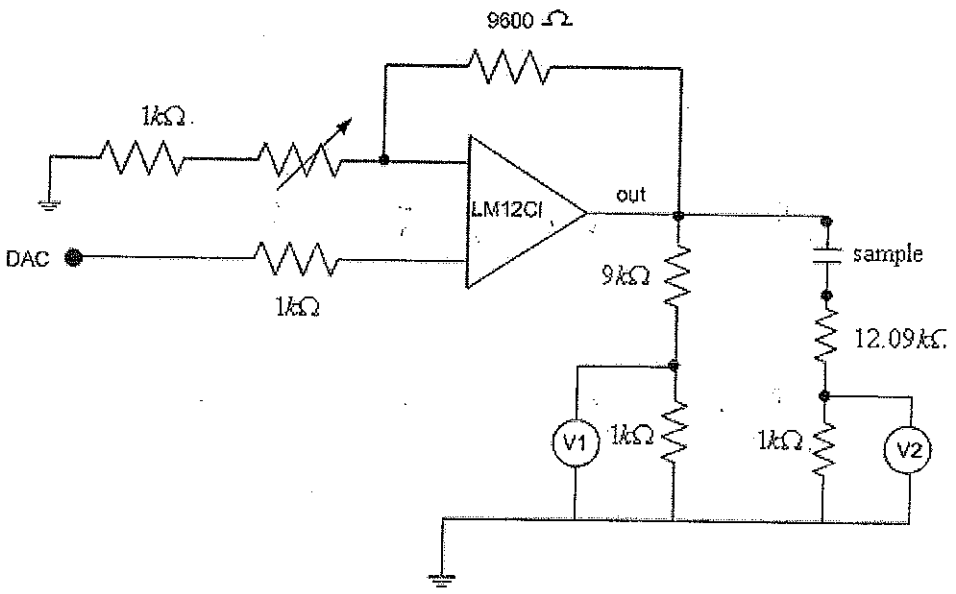

Figure 3.4. Voltage to voltage amplifier circuit.

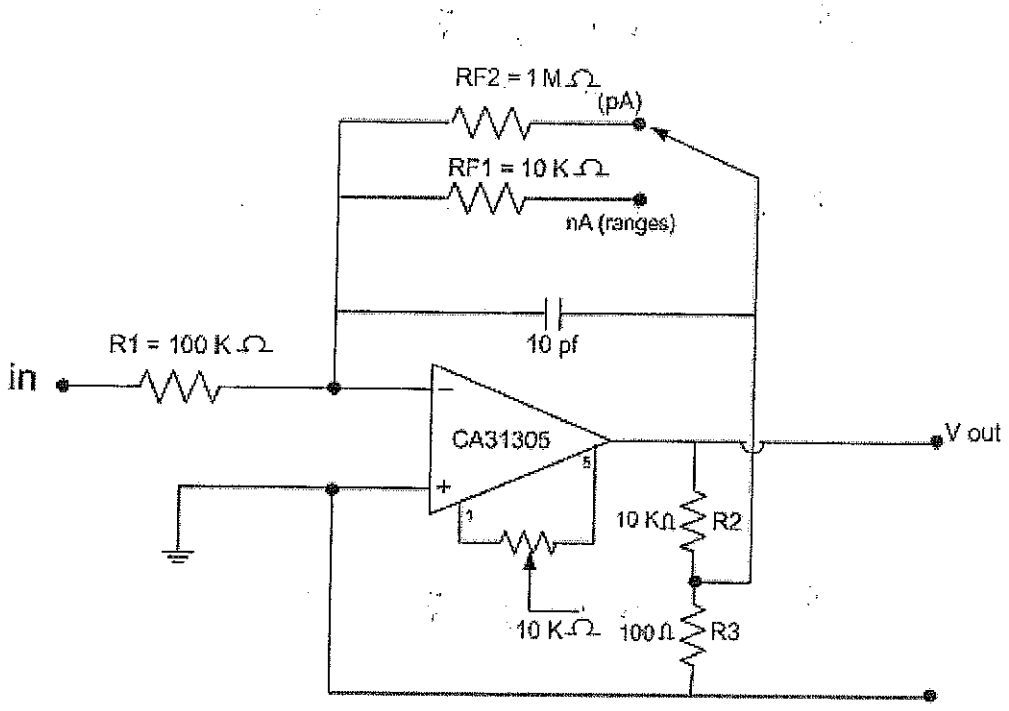

Figure 3.5. Current to voltage amplifier circuit.

3.5.2 Measurement of AC Electrical Conductivity

The AC electrical conductivity and loss tangent which is defined as the ratio of the imaginary or loss permittivity to the real permittivity of a material, were determined for the samples over a frequency range from $1kHz$ to $1MHz$. These measurements were taken at room temperature and at normal atmosphere pressure. The circiut used in these measurements is depicted in fig. 3.6. It consists of the following

1- A function generator (GFC 8055G) connected across the sample in series with a standard resistance R.

2- Tekronix TDS 360 dual–channel digital oscilloscope which was used to measure the total input voltage V_T and the potential drop across the standard resistance V_R.

The AC current passing through the sample and the resistance R is the same and can be calculated using Ohm's law

$$i = \frac{V_R}{R} \tag{3.3}$$

The values of loss tangent were obtained from the Lissajous figure displayed on the cathode ray oscilloscope screen. Referring to fig. 3.6, let V_X be the voltage applied to the X-channel and V_Y the voltage to the Y-channel.

If

$$V_X = V_T \sin(\omega t) \tag{3.4}$$

then

$$V_Y = V_R \sin(\omega t - \phi) \tag{3.5}$$

Where ϕ is the phase angle between the two potential V_X and V_Y, and ω is the angular frequency. These two signals form a Lissajous figure as shown in fig. 3.7. The position $V_Y = 0$, gives $V_X = V_\theta$. Also, for $V_Y = 0$, it implies that $(\omega t - \phi) = 0$ or $\omega t = \phi$. Therefore, we find that

$$V_\theta = V_T \sin(\pi - \phi) = V_T \sin(\phi) \tag{3.6}$$

$$\sin(\phi) = \frac{V_\theta}{V_T} \tag{3.7}$$

Hence, the loss tangent D or loss coefficient defined as the ratio of the imaginary or loss permittivity to the real permittivity of a material. It is given by

$$D = \tan\delta = \frac{\varepsilon''}{\varepsilon'} = \cot\phi \tag{3.8}$$

$$= \frac{\sqrt{(V_T^2 - V_\theta^2)}}{V_\theta} \tag{3.9}$$

Values of V_T and V_θ can be obtain directly from the oscilloscope screen, and the value of D at a given frequency can be calculated using equation (3-8).

3.5.3 Photovoltaic Effect Measurements

A schematic diagram of the experimental setup used to measure the photovoltaic effect is shown in fig. 3.2.b. A light beam from tungsten lamp was allowed to illuminate the sample through the transparent ITO electrode. The current and voltage were measured and recorded. Unfortunately, we don't have the capability to measure the light intensity falling on the sample in order to calculate the efficiency of the cell.

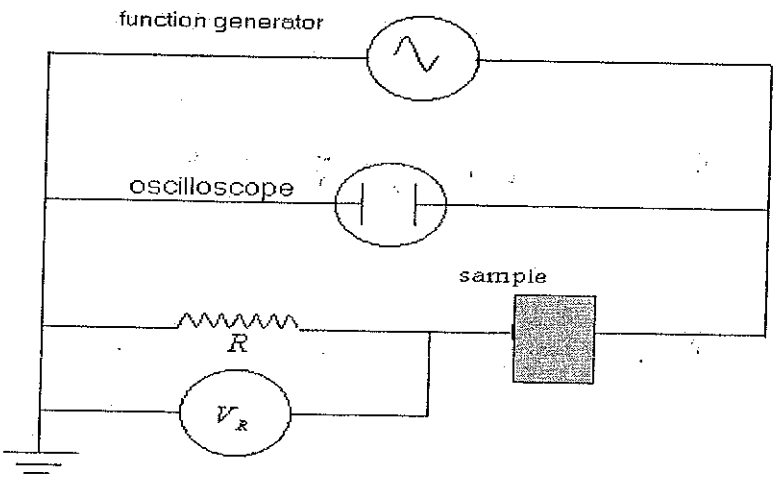

Figure 3.6. The circuit diagram used for AC conductivity measurements.

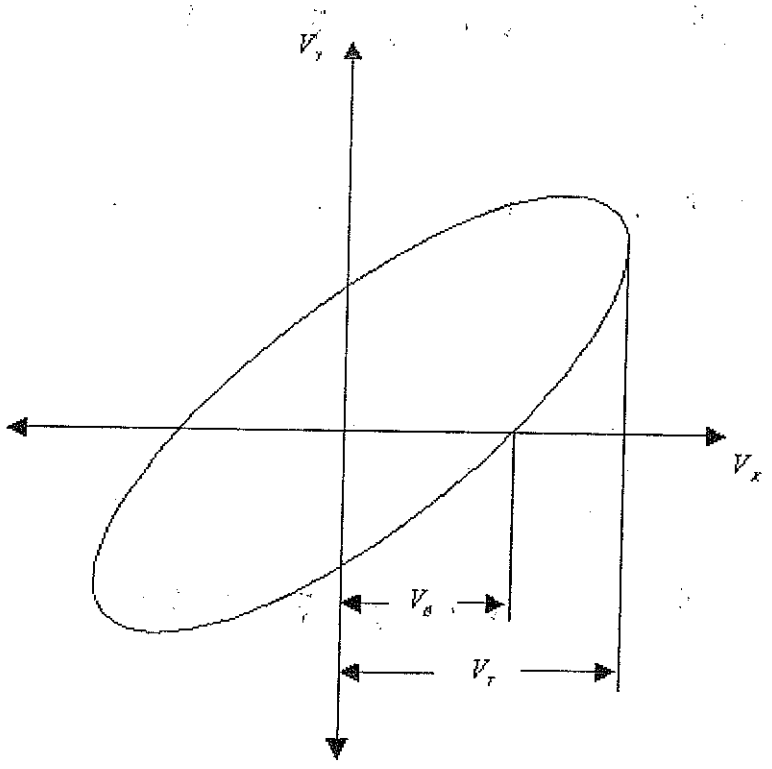

Figure 3.7. A typical Lissajous figure.

CHAPTER IV

RESULTS AND DISCUSSION

Results and discussion

4.1 Introduction

In this chapter, we present the experimental results and the discussion of our work. These results include the I-V characteristic curves for poly (9–vinylcarbazole) films doped with iodine. Also, the dependence of the DC current on the electric field, the sample thickness, the dopant level, and the temperature will be presented. The conduction mechanism will be discussed. Finally, additional measurements that include AC conductivity and photovoltaic measurements will be reported.

4.2 Results and Discussion

Poly (N-vinylcarbazole) can be considered as a prototype pendant group polymer. Its electronic properties, for instance the capability to transport optical excitations or charge carries, are all controlled by the dopant rather than main chain [5].

In this section, we discuss the results of our work performed on doped films of poly (9–vinylcarbazole).

4.2.1 DC I-V Characteristic Curves

Figure 4.1 through figure 4.3 depict the I–V characteristic curves of poly(9–vinylcarbazole) films doped with iodine at various dopant concentrations. It is clear from these figures that the current flowing through the sample (single layer) at low applied voltage increases slowly as the voltage increases. At higher voltages the rate of increase of current is much faster than

that at lower voltages. Moreover, when the polarity is reversed the current flowing through the sample shows similar behaviour.

4.2.2 Current–Electric Field Dependence

The relation between the natural logarithm of the measured current $\ln I$ and the square root of the applied electric field $E^{1/2}$ is shown in the fig. 4.4 through fig. 4.9. It is clear from these figures that these plots exhibit linear relationships; a slight deviation from this linear behaviour appears at the low applied electric field region. When the polarity is reversed the relationships for the current flowing through the sample and the electric field shows the same behaviour with different slopes. The slopes of these lines are shown in table 4.1 and table 4.2 for positive and negative ITO electrode respectively.

4.2.3 Conduction Mechanism

Figure 4.4 through fig. 4.9 show plots of the natural logarithm of the current against the square root of the applied electric field. These plots exhibit a linear relationship that can be illustrated by the following relation [5],

$$I\alpha \exp\left(\frac{e\beta E^{1/2}}{kT}\right) \qquad (4.1)$$

Where E is the applied electric field, e is the electronic charge, β is a constant characteristic of the conduction mechanism, k is Boltzmann's constant, and T is the absolute temperature. From the behavior depicted in these figures between $\ln I$ and $E^{1/2}$ the conduction mechanism could be determined. One can say that the charge carriers are released by thermal activation over a potential barrier. The physical nature of this potential barrier

may be interpreted in two different ways. First, it can be a transition of electrons over the potential barrier between the electrode and the polymer film (Schottky emission mechanism). Second, the charge carriers can be released from the traps into the sample film (Poole-Frenkel mechanism). In order to differentiate between these two conduction mechanisms the values of β were calculated from the slopes of $\ln I$ versus $E^{1/2}$ plots. The theoretical value of β can be calculated separately for either Poole-Frenkel or Schottky emission mechanism using the following equations

$$\beta_{PF} = \left(\frac{e}{\pi\varepsilon\varepsilon_0}\right)^{1/2} \tag{4.2}$$

For the Poole-Frenkel mechanism, and

$$\beta_{RS} = \frac{\beta_{PF}}{2} \tag{4.3}$$

For the Schottky emission mechanism, where ε_0 is the permittivity of free space, and ε is the dielectric constant of poly(9–vinylcarbazole) which equals to 3 [12]. The theoretical value of the Poole-Frenkel coefficient β_{PF} is $4.38\times10^{-5}\ V^{1/2}m^{1/2}$ and, the theoretical value of the Schottky coefficient β_{RS} is $2.19\times10^{-5}\ V^{1/2}m^{1/2}$. The experimental values of β are shown in table 4.1 and table 4.2 for various samples. It is clear that the experimental values of β is larger than the theoretical values of either "β_{PF} and β_{RS}". It also, in most cases, increases as the thickness of the films increases. The experimental values of β cannot determine the conduction mechanism because the experimental values are different from the theoretical values.

Jonscher and Carchano have suggested a proper way to draw a distinction between either Schottky or Poole-Frenkel mechanism [5]. The distinction between these mechanisms depends on the pre-exponential factors of equation 2.1 and equation 2.7 in chapter 2. These pre-exponential factors are

$$I_{OS} = RAT^2 \exp\left(-\frac{e\phi_{BP}}{kT}\right) \tag{4.4}$$

Where $e\phi_{BP}$ is the barrier height at the metal-insulator interface in the absence of a field in the case of schottky mechanism and

$$I_{OPF} = cAE \exp\left(-\frac{e\phi_{PF}}{kT}\right) \tag{4.5}$$

In the case of Poole-Frenkel mechanism. Here $e\phi_{PF}$ is the depth of the potential well.

Therefore, if one takes two electrodes of different work functions forming an asymmetric structure, the current will be very asymmetrical when one reverse the polarities in the case of Schottky mechanism. On the other hand, the current remains practically unchanged when one reverses the polarities in the case of Poole-Frenkel mechanism, which does not depend on the potential barrier between the electrodes and the bulk of the material.

It is clear from the plots of $\ln I$ versus $E^{1/2}$ for Al–film–ITO sandwich structure that the conduction depends on the polarities. It is obvious, from table 4.1 and table 4.2, that the slopes of the lines are different when the polarities are reversed. This indicates that the conduction in the films doped with different concentrations of iodine is Schottky mechanism (see section 2.2.1).

4.2.3 Activation Energy Measurement

The DC conductivity depends on the temperature. The DC conductivity arises from the thermal expansion of the material and the phonon contributions to the self-energy of the electrons [5]. The measurements were taken at various temperature (between $300K$ to $400K$). At each data point the temperature of the sample was allowed to stabilize for several minutes. Figure 4.10.a shows the variations of the I-V curves with temperature for a sample doped with 1% iodine. This figure illustrates that the DC conductivity of all samples increases with increasing temperature. The relation between $\ln I$ versus $E^{1/2}$ for the same sample doped with 1% I_2 at different temperature is illustrated in fig. 4.10.b. It is clear from the figure that these plots exhibit linear relationships. Figure 4.11 through fig. 4.17 show plots of the natural logarithm of the DC conductivity against the reciprocal of temperature. In these measurements the applied voltage was kept fixed at 14, 18, 20 and 22 volt respectively. The resistance of the sample was calculated from the relation

$$R = \frac{V}{I} \tag{4.6}$$

The DC conductivity was calculated using the following relation

$$\sigma = \frac{IL}{VA} \tag{4.7}$$

Where σ is the DC conductivity, L is the film thickness, and A is the electrode area. The relation between the DC conductivity and the temperature in films doped with different concentrations of iodine I_2 is shown in fig. 4.11

through fig. 4.17. It is clear that these figures exhibit linear relationships. This behavior indicates that the DC conductivity σ obeys the following relation

$$\sigma = \sigma_0 \exp\left(-\frac{\varepsilon_a}{kT}\right) \tag{4.8}$$

Where σ_0 is the maximum conductivity, and ε_a is the activation energy. Table 4.3 lists values of ε_a for various single layer samples at different dopant weight concentrations. These values of ε_a indicate a typical electronic conduction [34].

4.2.4 Thickness Dependence

The current dependence on the thickness of poly(9–vinylcarbazole) films doped with iodine at various dopant concentrations is apparent in fig. 4.18 through fig. 4.20. These data were taken from the I-V characteristic curves by fixing the value of the square root of applied electric field $E^{1/2}$ to 1400 ,1600, 1800, and 2000 $(V/m)^{1/2}$. These graphs show that the current flowing through a sample decreases as the film thickness increases, and the current flowing through thinner films is several times higher than the current flowing through thicker ones. This behavior indicates that the conduction electrons experience more difficulty in flowing through thicker films than flowing through thinner ones. Figure 4.21 shows that the current flowing through films with different thicknesses and doped with iodine increases as the dopant weight concentration increases. Figure 4.22 depicts the variation of current with dopant concentration at constant thickness (5.5 μm, 6 μm, 7μm).

4.3 Additional Measurements

4.3.1 AC Electrical Conductivity Measurements

The variation of the *AC* conductivity with the frequency in the range from $1KHz$ up to $3MHz$ was studied for samples of the poly(9–vinylcarbazole) films doped with different iodine weight concentrations as indicated in table 4.1. These measurements were taken at room temperature and in normal atmosphere. Figure 4.23 depicts the variation of current with frequency. It is clear from these figures that the current flowing through the sample at frequencies higher than $1KHz$ increases fast. At frequencies higher than $0.5MHz$ the current starts to increase slowly. All samples exhibit the same behavior with the variation of the applied frequency. The relation between $\tan\delta$ and frequency is shown in fig. 4.23.b. The current density J through the sample is given by

$$J = \sigma E \tag{4.9}$$

Where σ is the conductivity and E is the electric field. Thus, the conductivity is given by

$$\sigma = \frac{J}{E} = \frac{I/A}{V/d} \tag{4.10}$$

Where A is the area of the sample electrode and V is the applied voltage. Figure 4.24 shows the variation of conductivity σ with frequency.

4.3.2 I-V Characteristic Curves for Double Layer Films

The I–V characteristics for a double layer film arrangement ITO-poly (9-vinylcarbazole)-Rhodamine 6G-Al electrode is illustrated in fig. 4.25. It is

clear from this figure that the current flowing through the sample at low applied voltage increases slowly as the applied voltage increases. At higher voltages the rate of increase of current is faster than at lower voltages when the ITO electrode is negative. When the polarity is reversed (ITO electrode is positive) the I-V characteristic curves show the same behaviour with lower current flowing through the sample. We found that such behaviour is more pronounced in the case of disimilar electrode (Al-sample-ITO) than the case of samples with similar electrodes (Al-sample-Al) as shown in fig.4.26. This indicates that the conduction mechanism is most probably Schottcky mechanism.

Figure 4.27 and fig. 4.28 show the relation between the natural logarithm of the current and the square root of applied voltage $V^{1/2}$. This indicates that the conduction mechanism in these films obeys Schottcky mechanism (see section 4.2.3).

4.3.3 Photovoltaic Effect for Double Layer Film

It was found that poly(9-vinylcarbazole)–iodine complex exhibits photovoltaic effect when illuminated with light [18,24]. We found that the double layer sample described in section 3.2 exhibits this effect.

Figure 4.29 shows the I-V characteristic curve for our sample. This confirms the existence of photovoltaic effect in our sample though it is rather weak compared with that of a silicon cell. In order to further investigate this effect, the output power of the illuminated sample was calculated. Figure 4.30

illustrates the output power verses voltage. The maximum power was attained at an output voltage of 5.26mV.

The curve factor (c.f.) is defined as the ratio between the biggest rectangle inside the curve and the smallest one outside it is given by

$$c.f. = \frac{I_{\max} V_{\max}}{I_{sc} V_{oc}} \tag{4.11}$$

Where I_{sc} and V_{oc} are the short circuit current and open circuit voltage respectively. The curve factor for our sample was found to be equal to 0.54.

The photovoltaic may be explained as follows: The sample absorb light at energies above the band gap, leading to the separation of positive and negative charge carriers. These carriers are collected at opposite electrodes. Upon increasing the light intensity more electron–hole pairs will be created and separated, and, thus the greater will be the potential difference across the electrodes of the film.

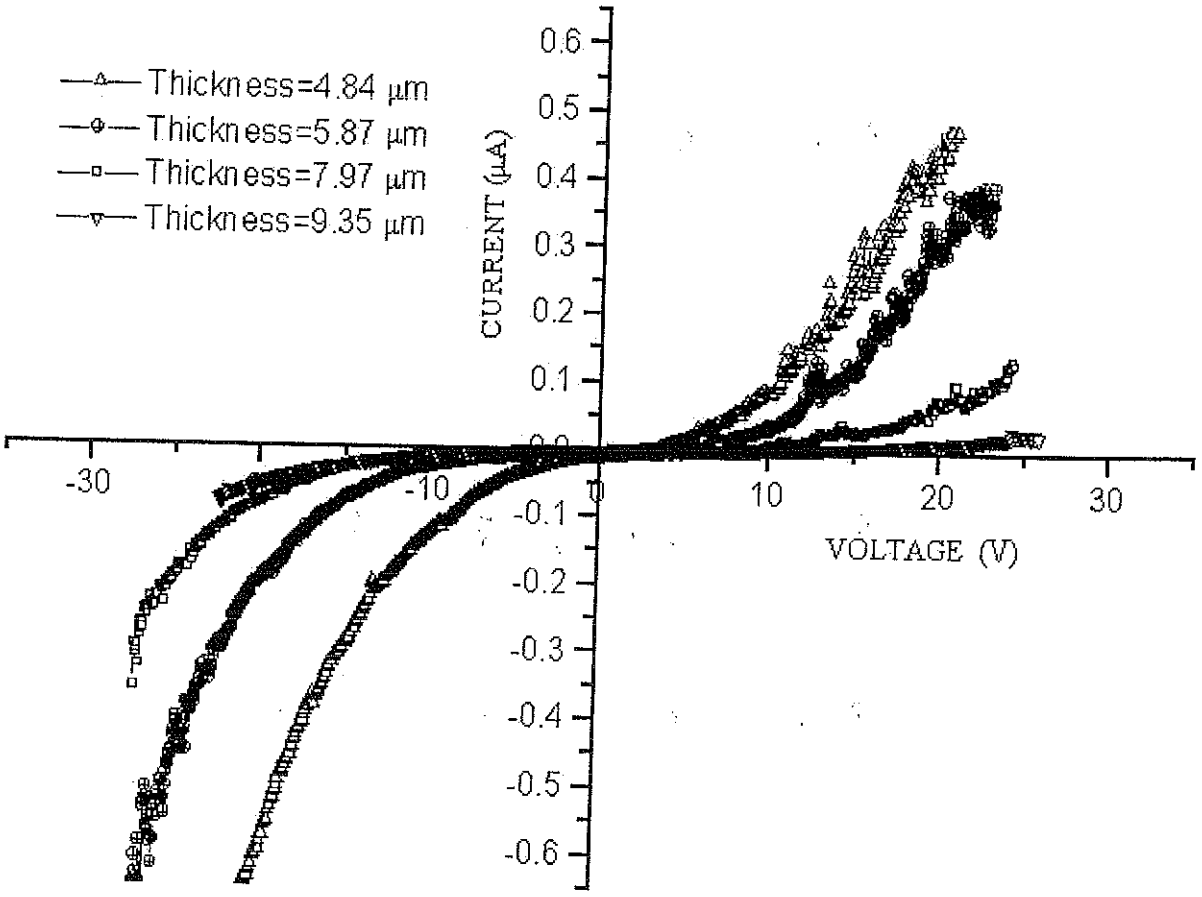

Figure 4.1. I-V characteristic curves for single layer poly (9-vinylcarbazole) films doped with 1.0% I_2.

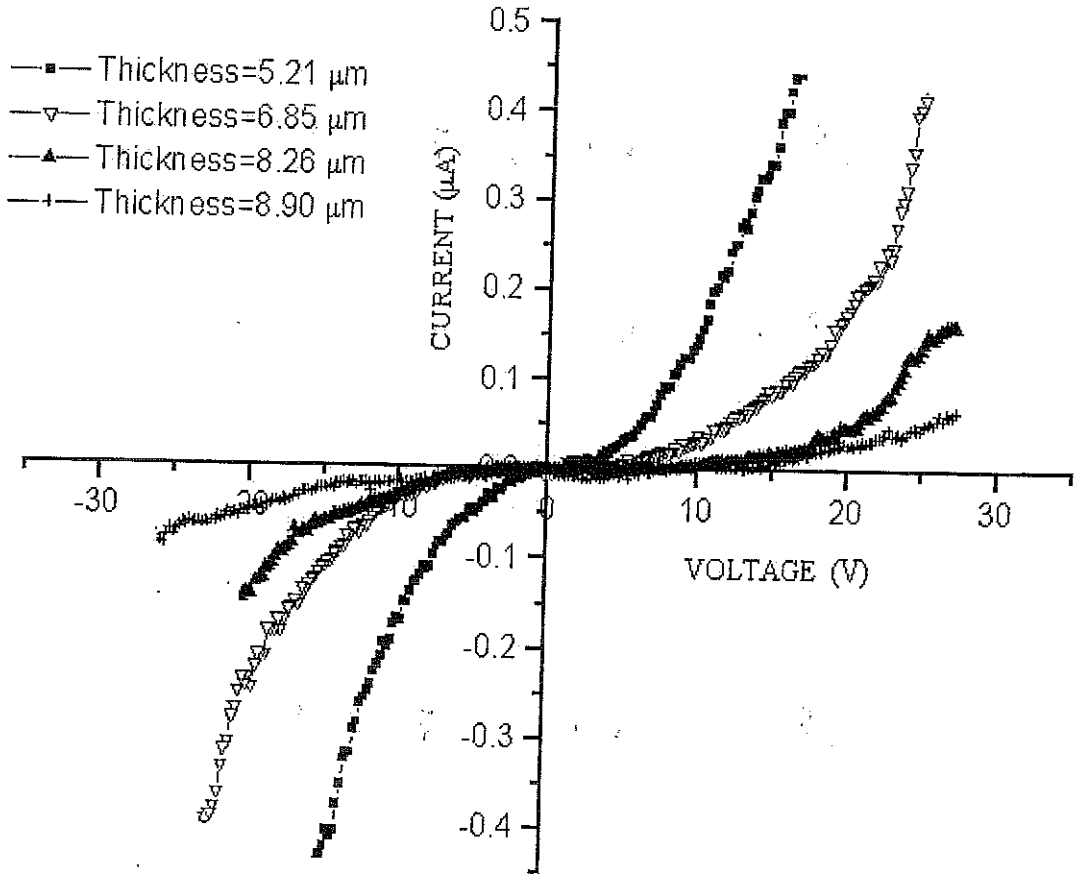

Figure 4.2. I-V characteristic curves for single layer poly (9-vinylcarbazole) films doped with 2.0% I_2.

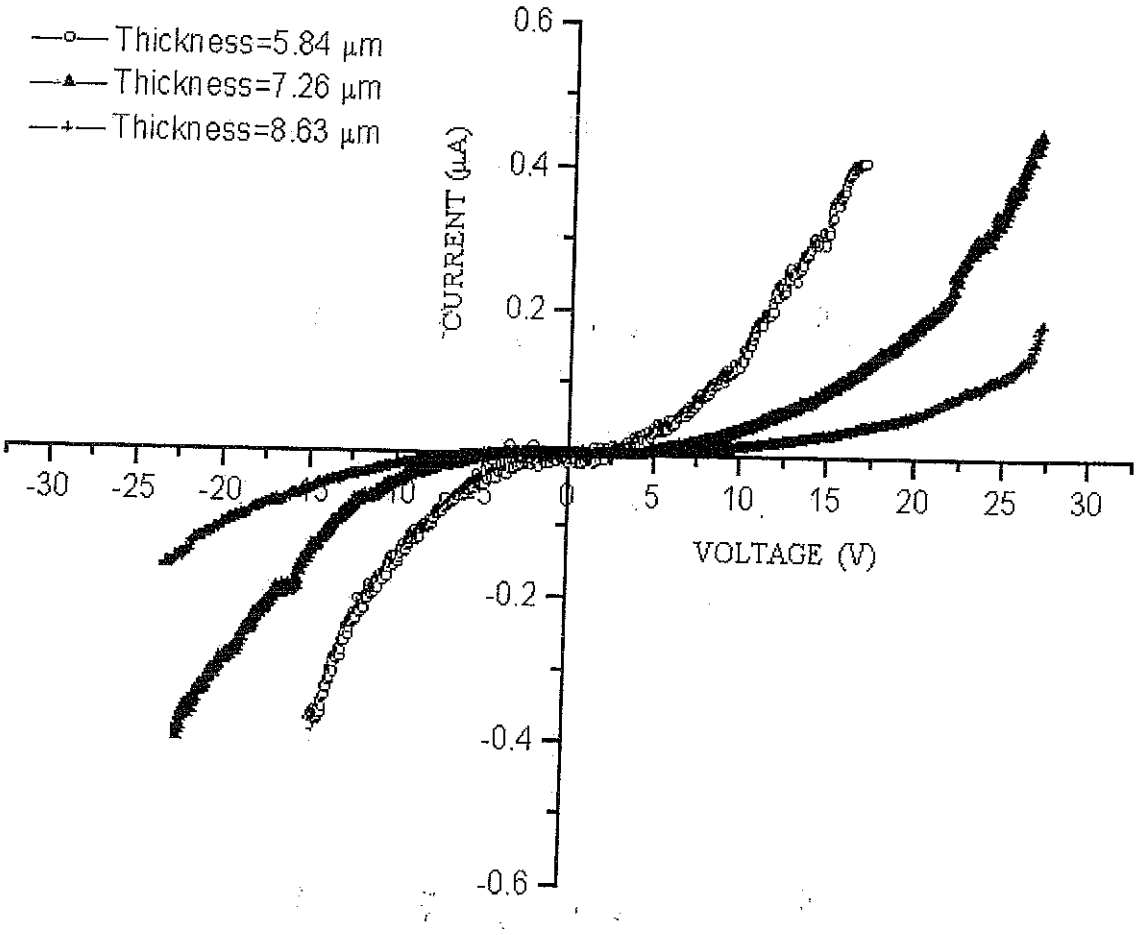

Figure 4.3. I-V characteristic curves for single layer poly (9-vinylcarbazole) films doped with 4.0% I_2.

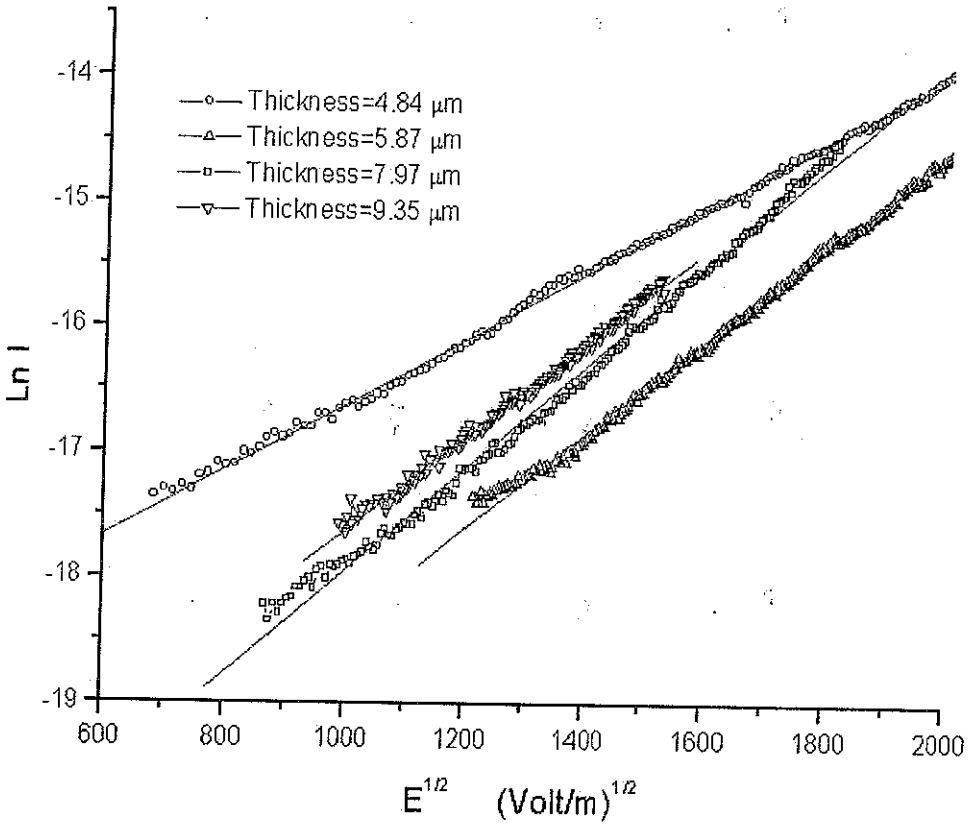

Figure 4.4. Plots of natural logarithm of the current versus square root of applied electric field for films doped with 1.0% I_2; ITO electrode is positive.

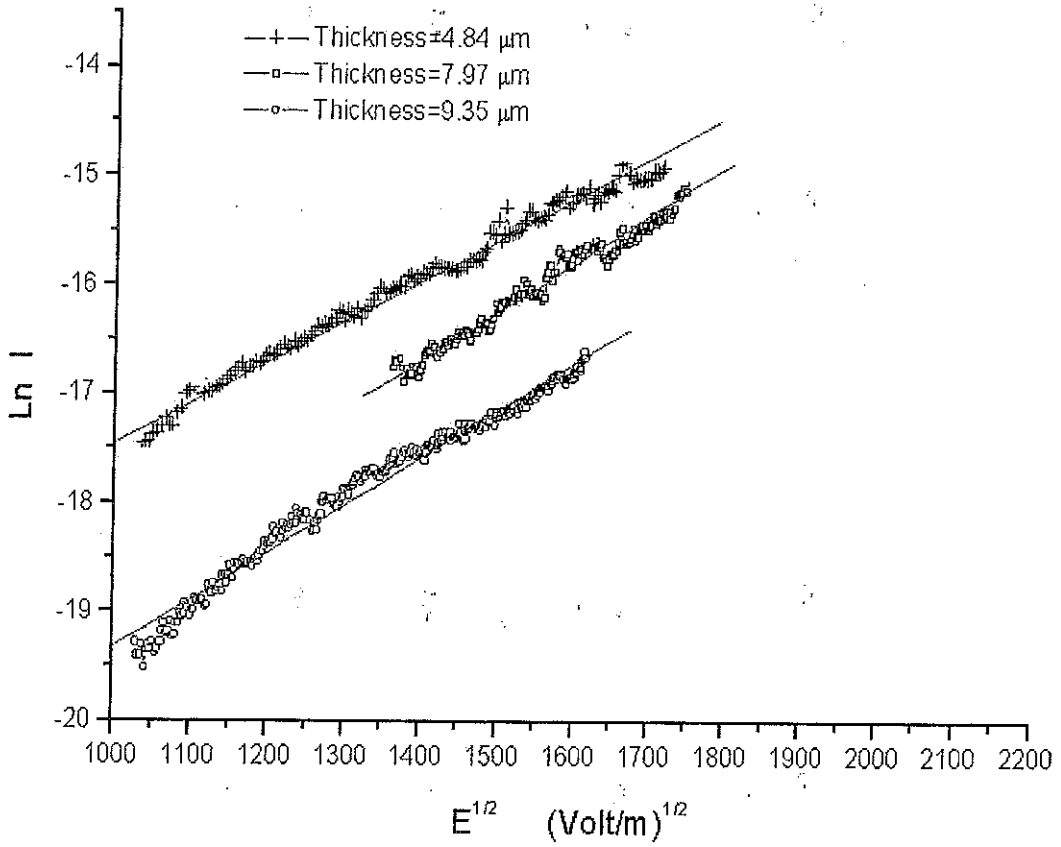

Figure 4.5. Plots of natural logarithm of the current versus square root of applied electric field for films doped with 1.0% I_2; ITO electrode is negative.

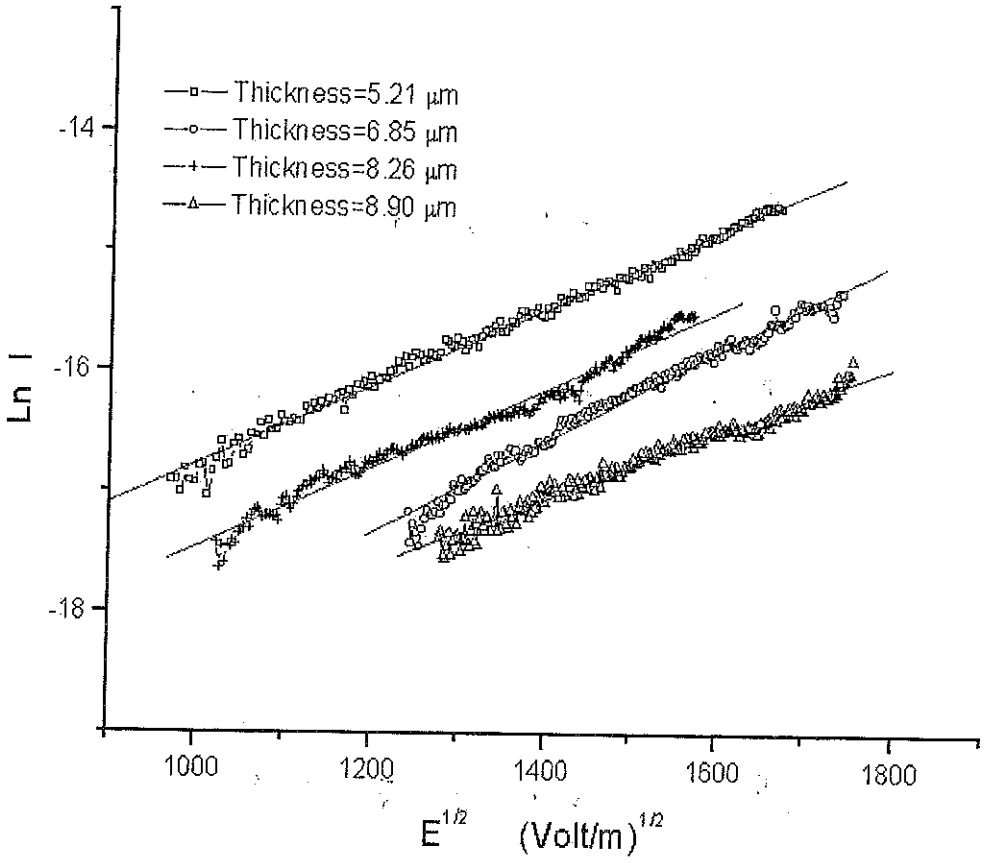

Figure 4.6. Plots of natural logarithm of the current versus square root of applied electric field for films doped with 2.0% I_2; ITO electrode is positive.

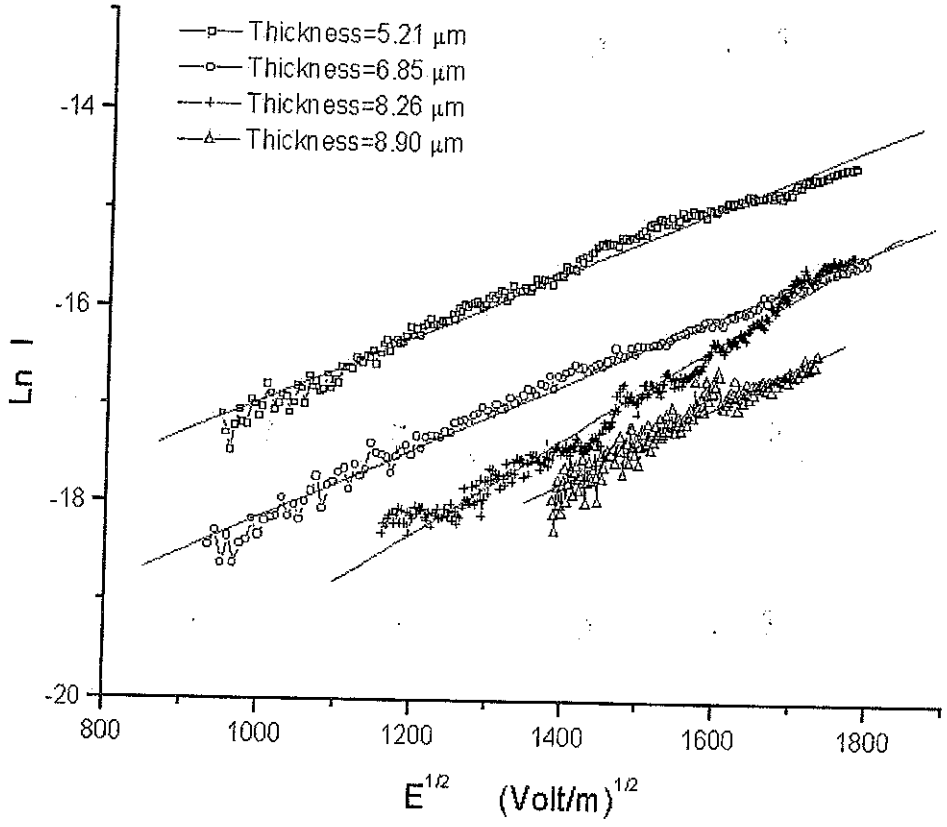

Figure 4.7. Plots of natural logarithm of the current versus square root of applied electric field for films doped with 2.0% I_2; ITO electrode is negative.

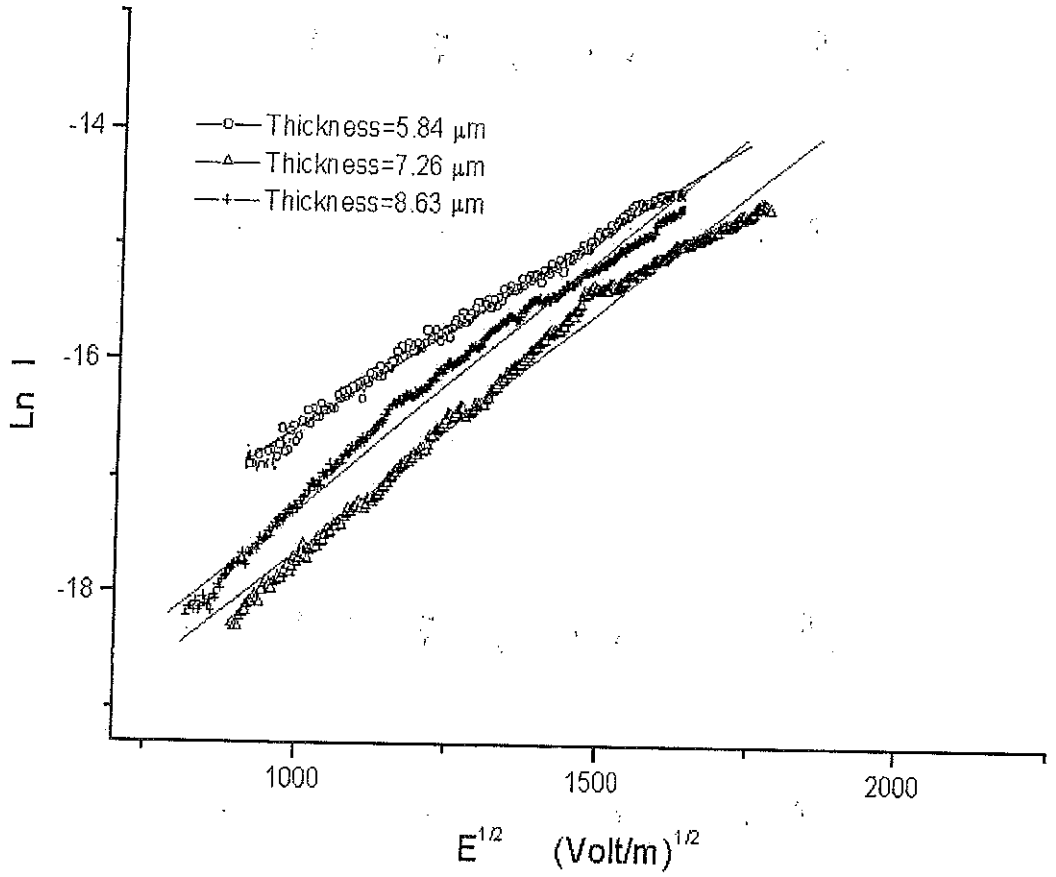

Figure 4.8. Plots of natural logarithm of the current versus square root of applied electric field for films doped with 4.0% I_2; ITO electrode is positive.

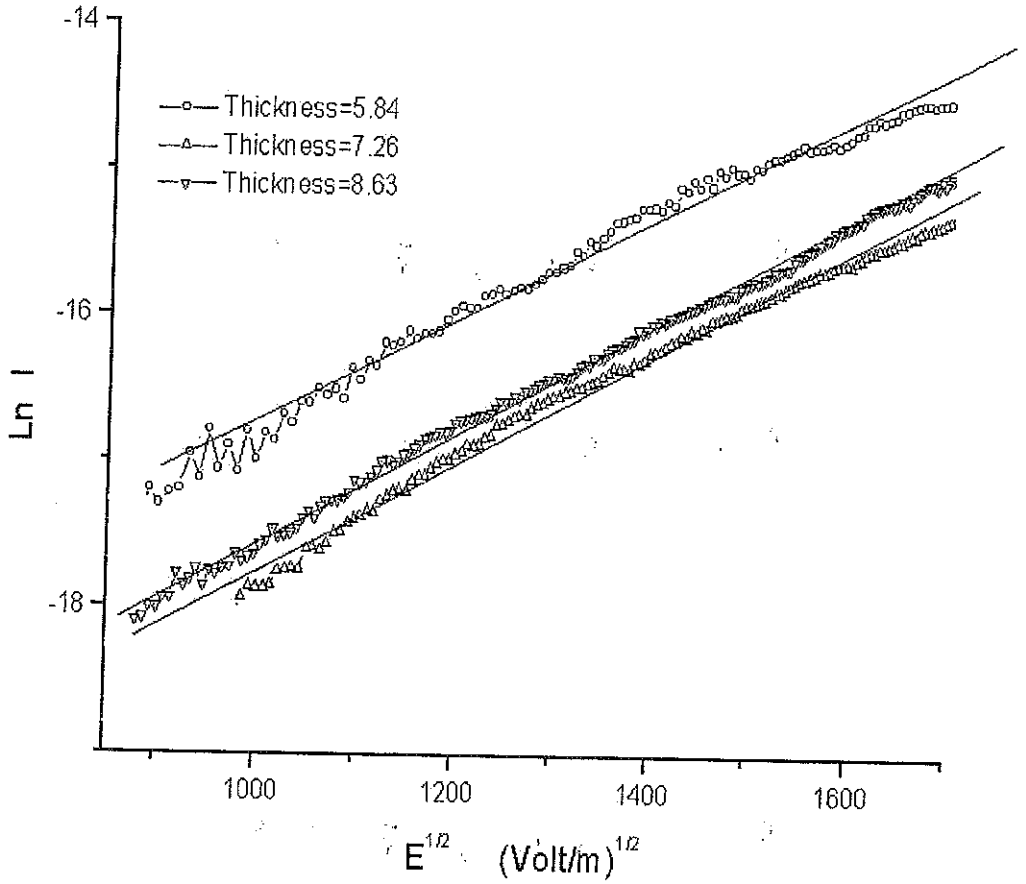

Figure 4.9. Plots of natural logarithm of the current versus square root of applied electric field for films doped with 4.0% I_2; ITO electrode is negative.

Sample	Thickness (μm)	Slope x 10^{-3}	β $(V^{1/2}m^{1/2})x10^{-5}$
1.0% iodine doped poly (9-vinylcarbazole)	4.84μm	2.49	6.43
	5.87μm	2.74	7.08
	7.97μm	4.34	11.21
	9.35μm	3.31	8.55
2.0% iodine doped poly (9-vinylcarbazole)	5.21μm	4.29	11.08
	6.85μm	2.06	5.32
	8.26μm	2.59	6.61
	8.90μm	4.08	10.54
4.0% iodine doped poly (9-vinylcarbazole)	5.84μm	3.52	9.09
	7.26μm	4.45	11.49
	8.63μm	4.6	11.88

Table 4.1. Experimental values of β and slopes of lines for samples at different thickness, ITO electrode is positive.

Sample	Thickness (μm)	Slope x 10^{-3}	β $(V^{1/2}m^{1/2})x10^{-5}$
1.0% iodine doped poly (9-vinylcarbazole)	4.84μm	3.65	9.43
	7.97μm	4.27	11.03
	9.35μm	4.44	11.47
2.0% iodine doped poly (9-vinylcarbazole)	5.21μm	3.71	9.58
	6.85μm	3.87	9.97
	8.26μm	5.57	14.39
	8.90μm	5.6	14.46
4.0% iodine doped poly (9-vinylcarbazole)	5.84μm	4.21	10.87
	7.26μm	4.48	11.57
	8.63μm	4.62	11.93

Table 4.2. Experimental values of β and slopes of lines for samples at different thickness, ITO electrode is negative.

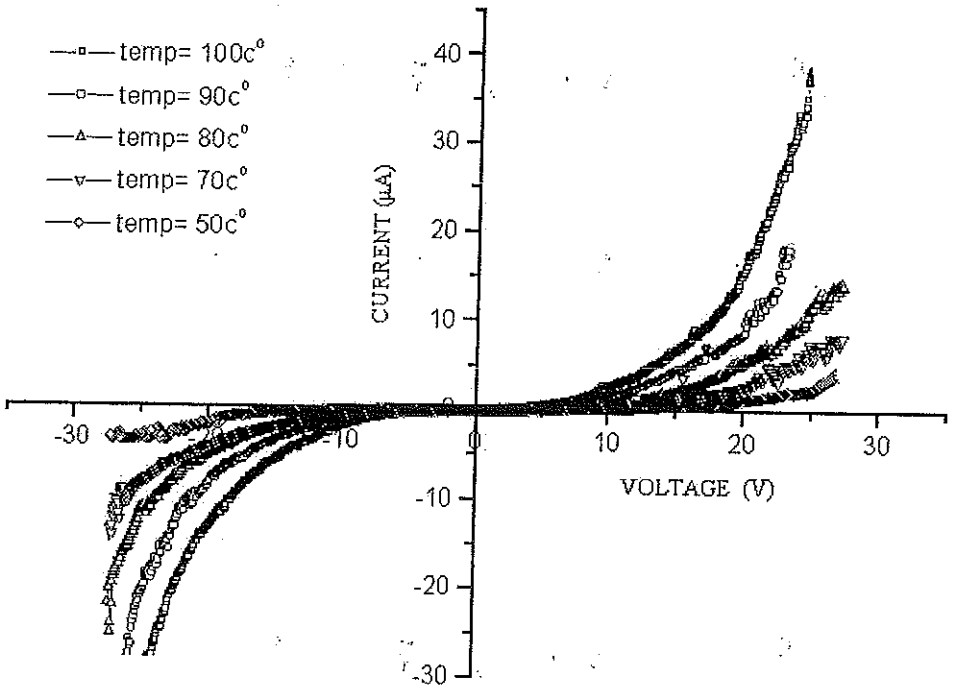

(a)

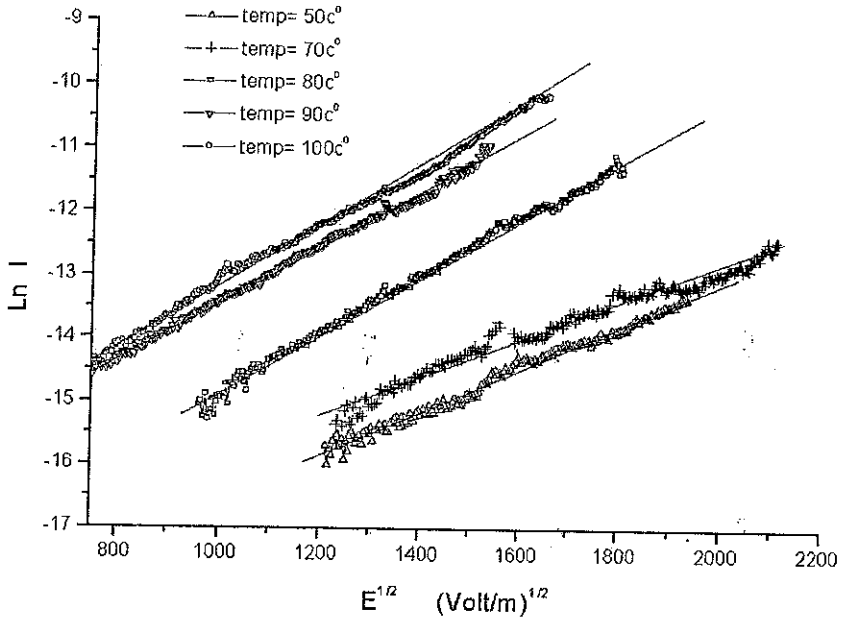

(b)

Figure 4.10.(a) Shows the change of I-V curve with for film doped with I_2 different temperature (b) Plots of natural logarithm of the current versus square root of applied electric field for films doped with I_2 different temperature.

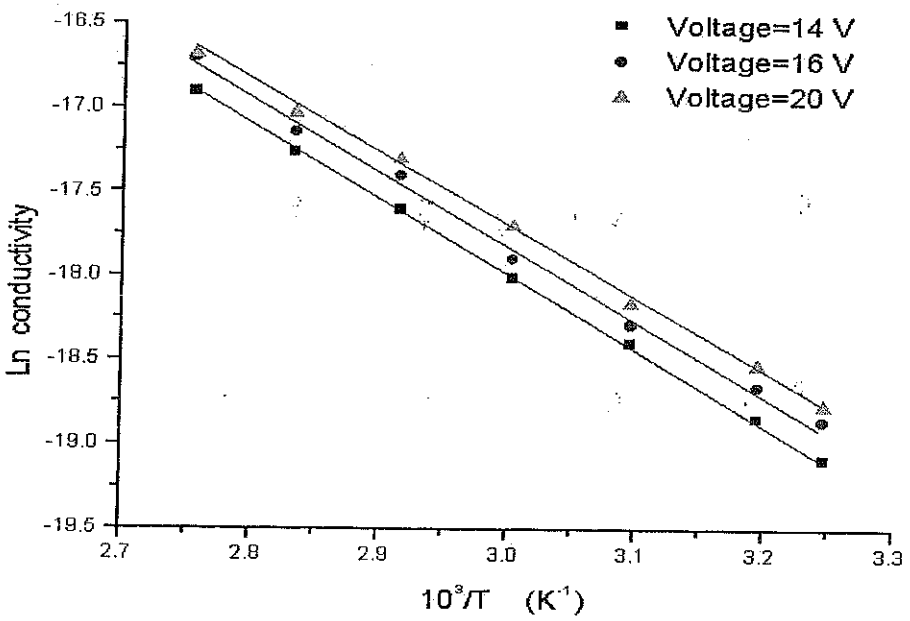

Figure 4.11. The natural logarithm of DC conductivity versus temperature (1000/T) for film doped with 1.0% I_2 and thickness 9.35 μm.

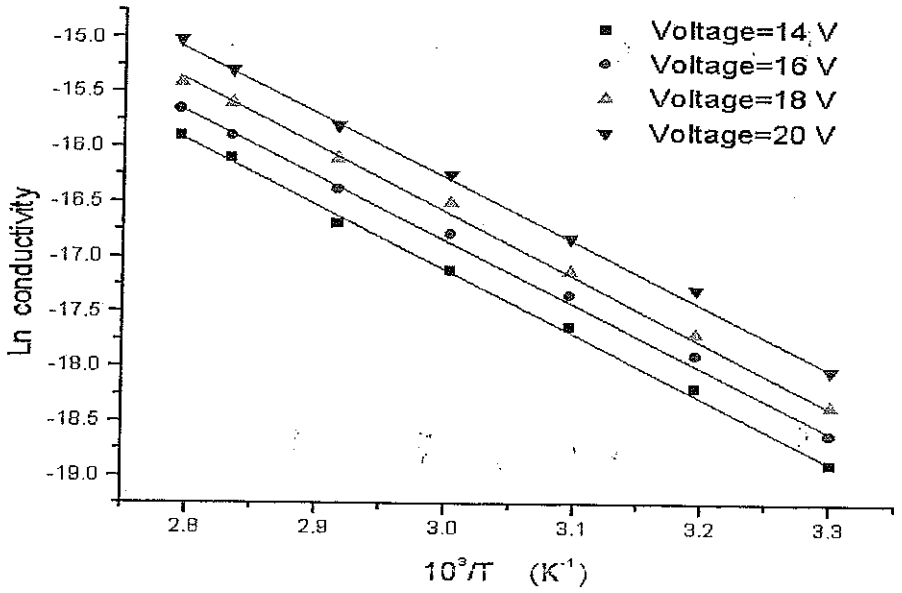

Figure 4.12. The natural logarithm of DC conductivity versus temperature (1000/T) for film doped with 1.0% I_2 and thickness 4.84 μm.

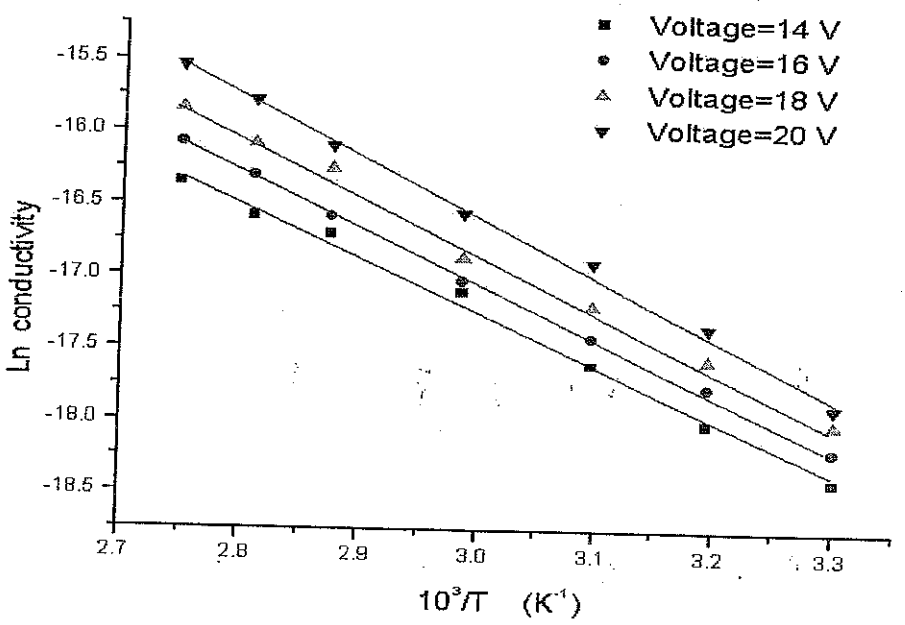

Figure 4.13. The natural logarithm of DC conductivity versus temperature (1000/T) for film doped with 1.0% I_2 and thickness 7.97 μm.

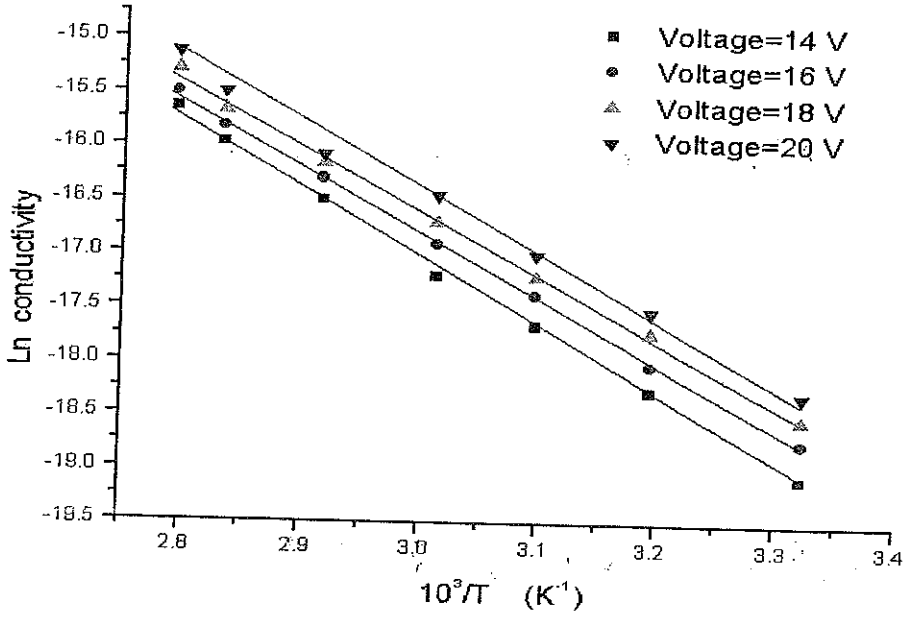

Figure 4.14. The natural logarithm of DC conductivity versus temperature (1000/T) for film doped with 2.0% I_2 and thickness 8.26 μm.

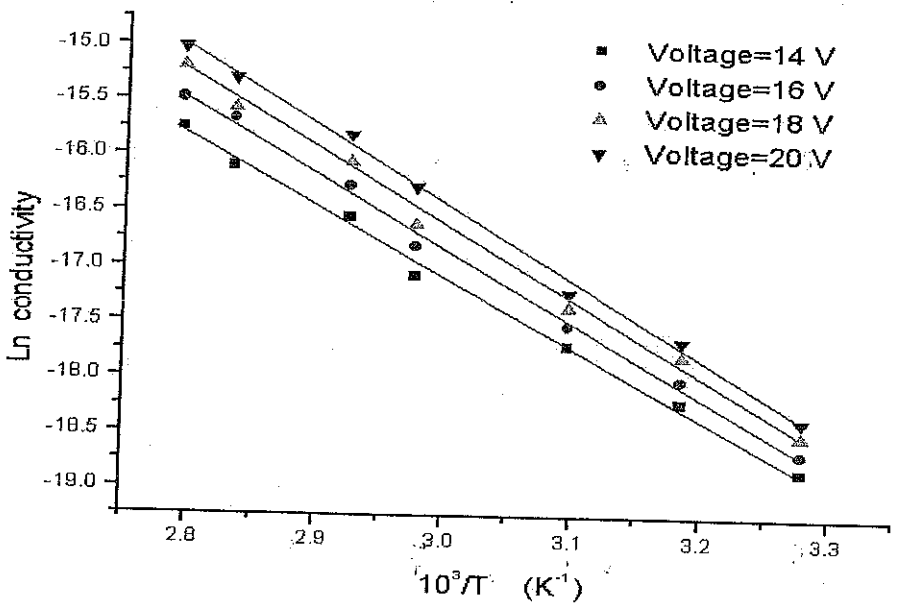

Figure 4.15. The natural logarithm of DC conductivity versus temperature (1000/T) for film doped with 2.0% I_2 and thickness 6.85 μm.

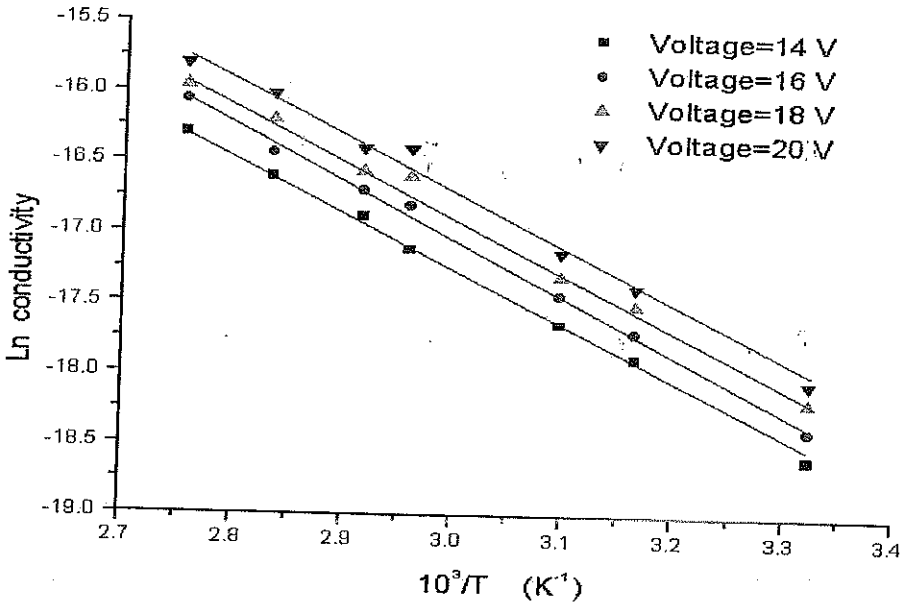

Figure 4.16. The natural logarithm of DC conductivity versus temperature (1000/T) for film doped with 2.0% I_2 and thickness 5.21 μm.

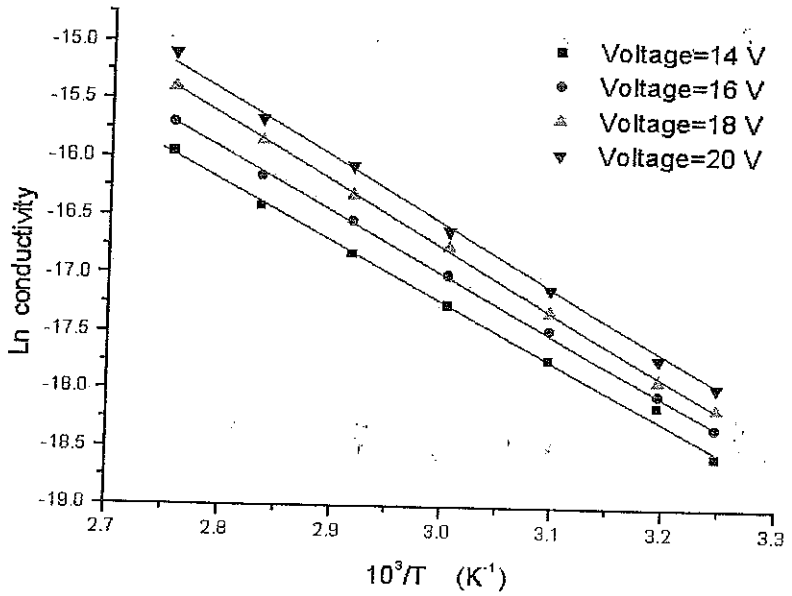

Figure 4.17. The natural logarithm of DC conductivity versus temperature (1000/T) for film doped with 4.0% I_2 and thickness 5.84 μm.

Sample	Thickness (μm)	Activation energy ε_a (eV)
1.0% iodine doped poly (9-vinylcarbazole)	4.84μm	0.473
	5.87μm	0.456
	7.97μm	0.332
	9.35μm	0.357
2.0% iodine doped poly (9-vinylcarbazole)	5.21μm	0.556
	6.85μm	0.544
	8.26μm	0.478
	8.90μm	0.441
4.0% iodine doped poly (9-vinylcarbazole)	5.84μm	0.451
	7.26μm	0.531
	8.63μm	0.486

Table 4.3. Experimental values of the activation energy ε_a for samples at different thickness and different dopant weight concentrations.

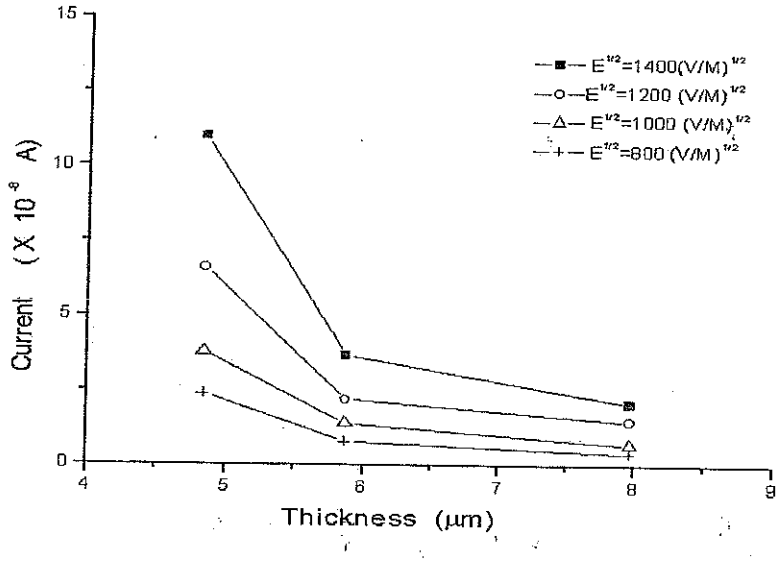

(a)

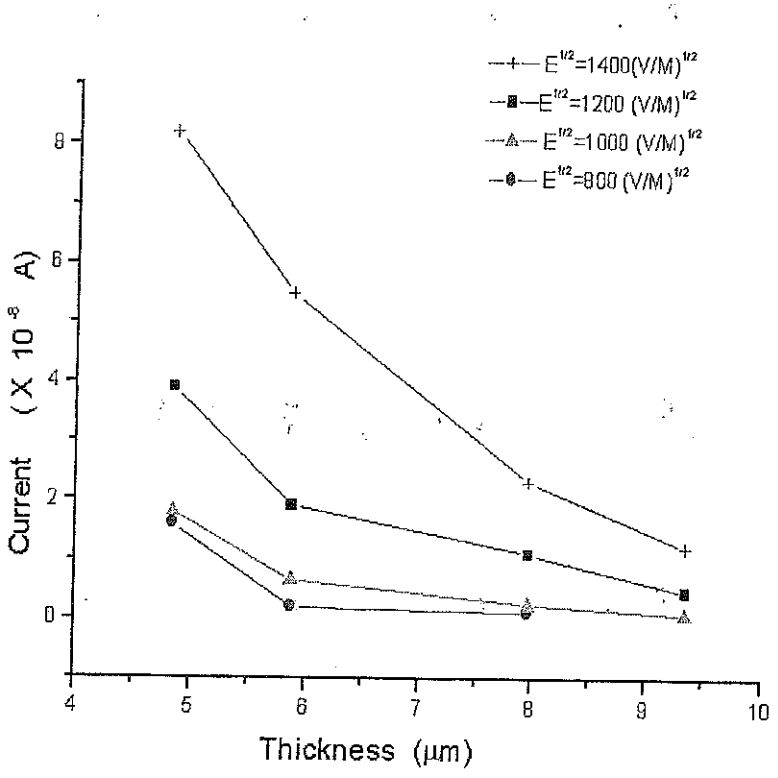

(b)

Figure 4.18. Variation of current with film thickness at I_2 concentration 1% at various applied electric field, (a) ITO electrode is positive, and (b) ITO electrode is negative.

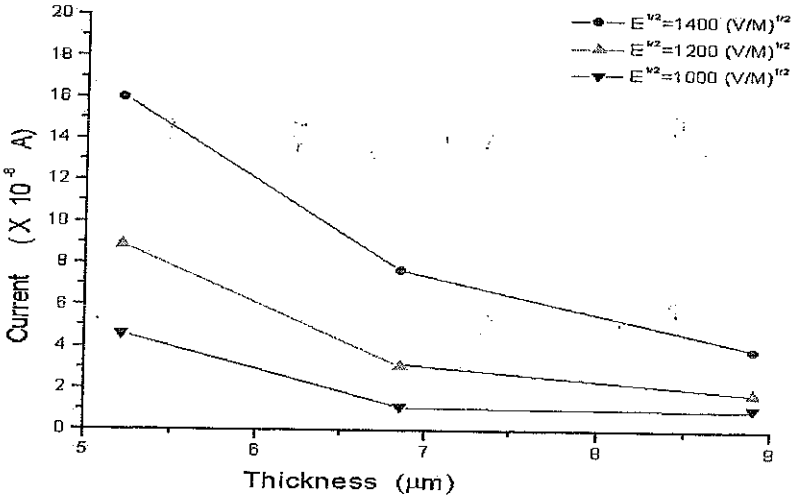

(a)

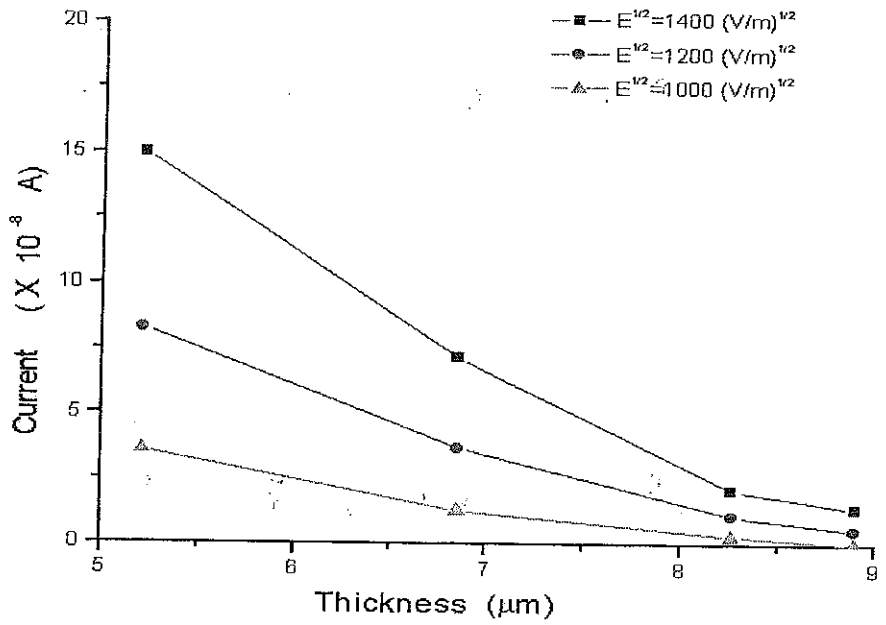

(b)

Figure 4.19. Variation of current with film thickness at I_2 concentration 2% at various applied electric field, (a) ITO electrode is positive and (b) ITO electrode is negative.

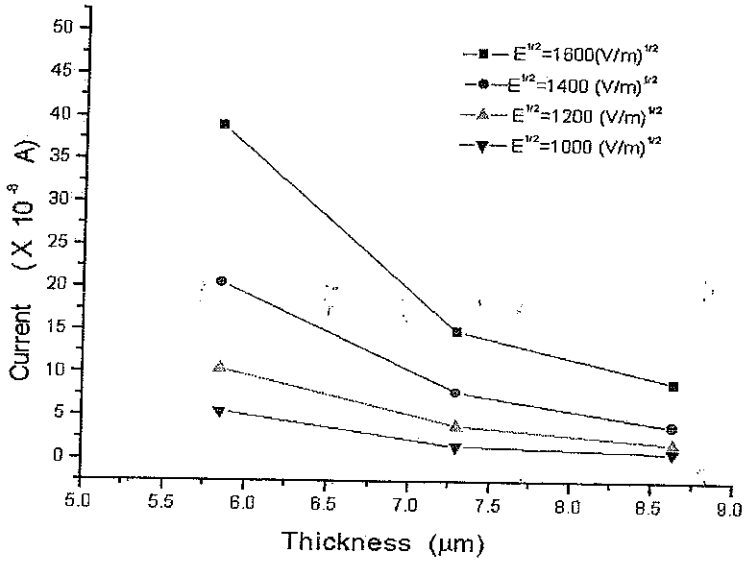

(a)

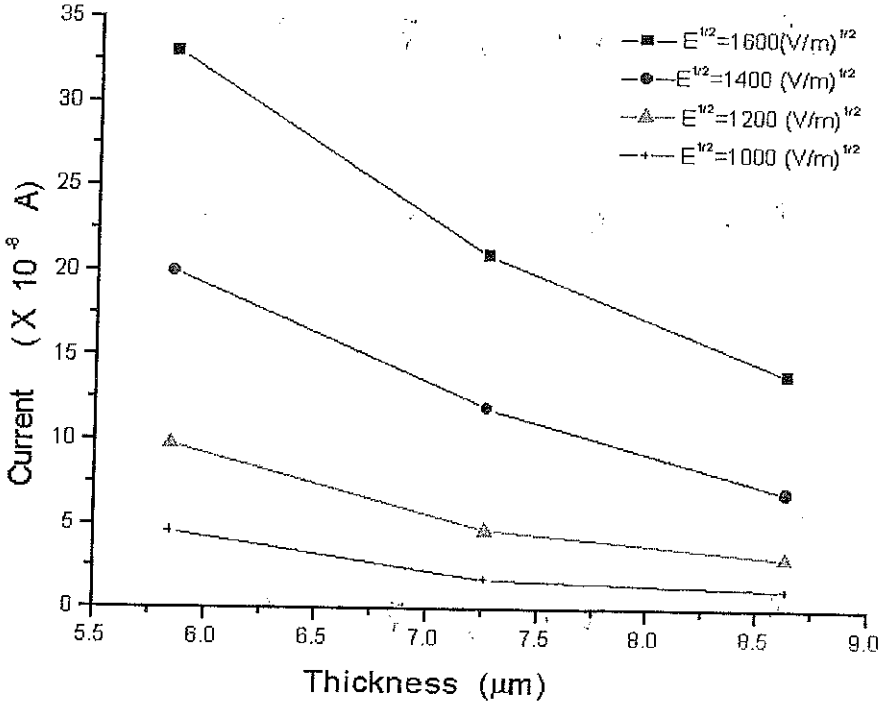

(b)

Figure 4.20. Variation of current with film thickness at I_2 concentration 4% at various applied electric field, (a) ITO electrode is positive and (b) ITO electrode is negative.

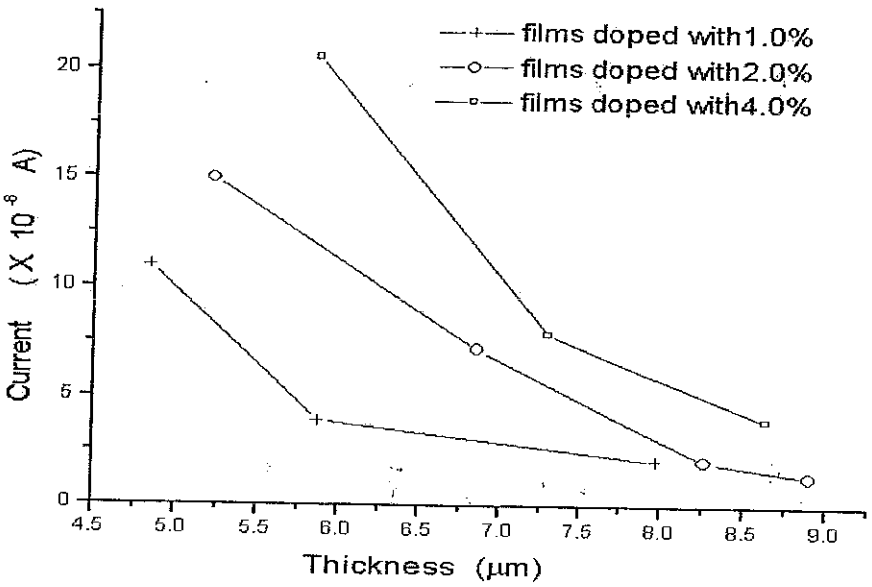

Figure 4.21. Variation of current with film thickness at various dopent concentration.

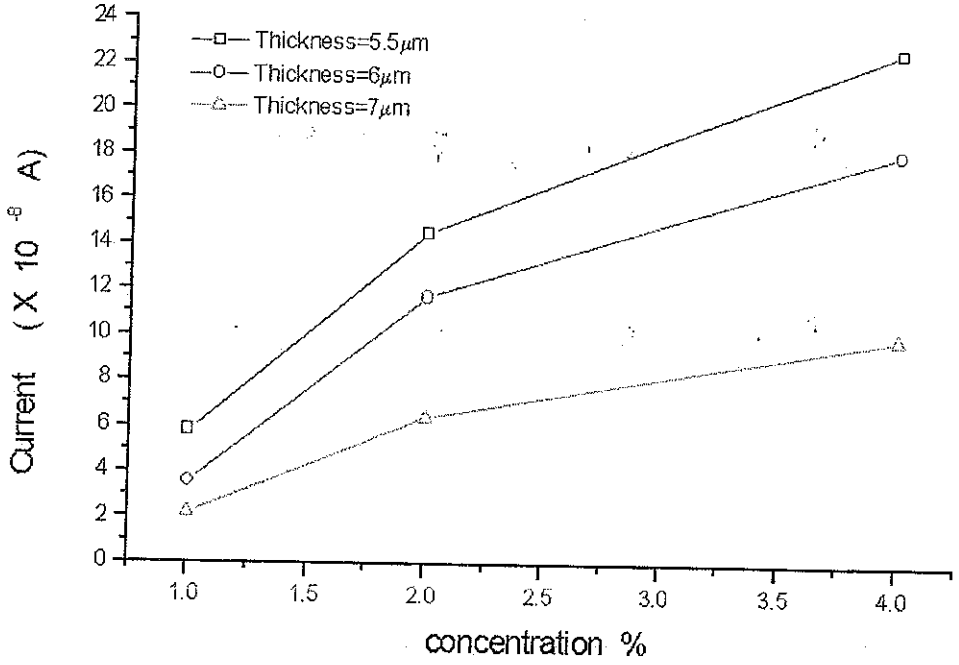

Figure 4.22. Variation of current with concentration for different the film thickness.

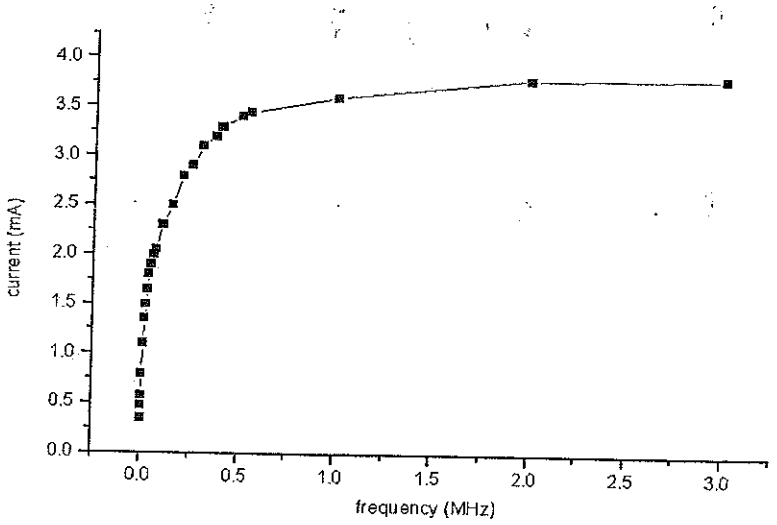

(a)

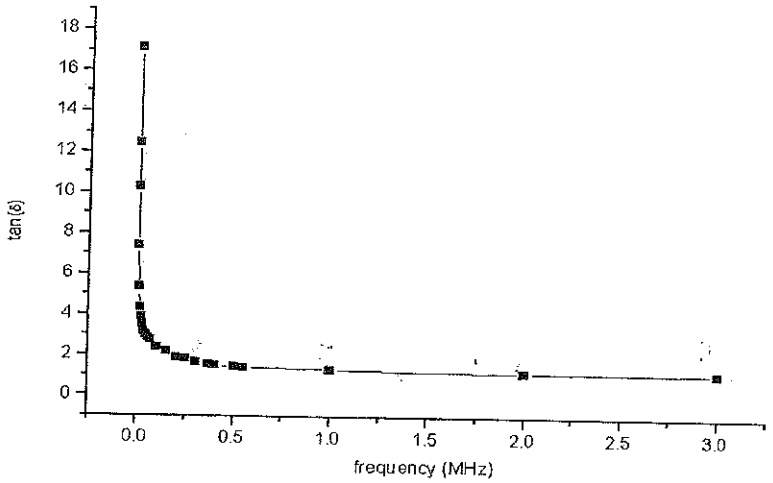

(b)

Figure 4.23. (a) A Plot of current versus the applied frequency, (b) A Plot of $\tan(\delta)$ against the applied frequency for the film doped 2% of I_2 and thickness 6.85μm.

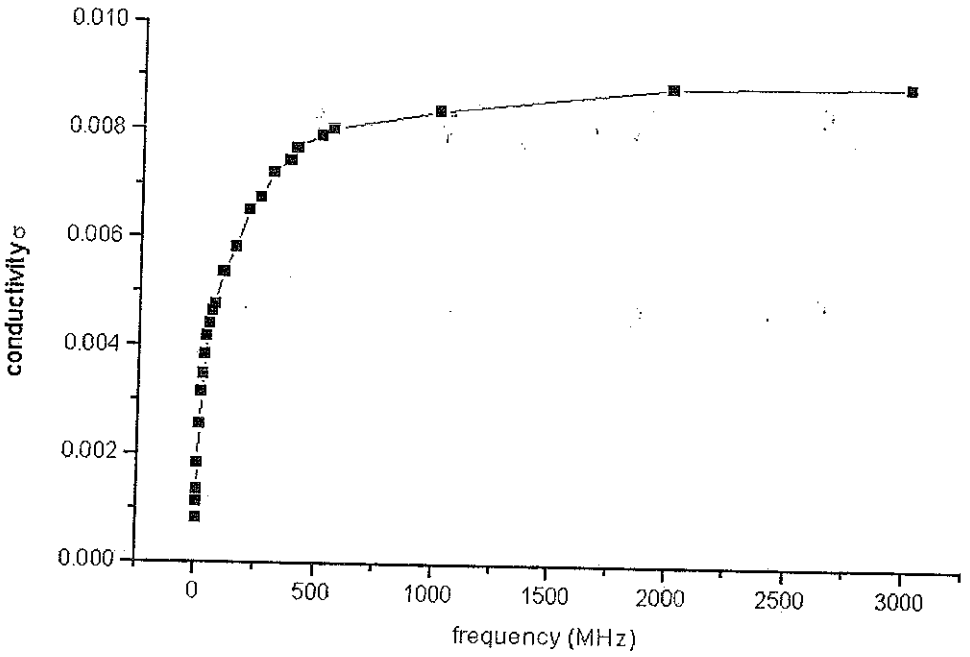

Figure 4.24 A Plot of AC conductivity σ versus the applied frequency for the film doped 2% of I_2 and thickness 6.85μm.

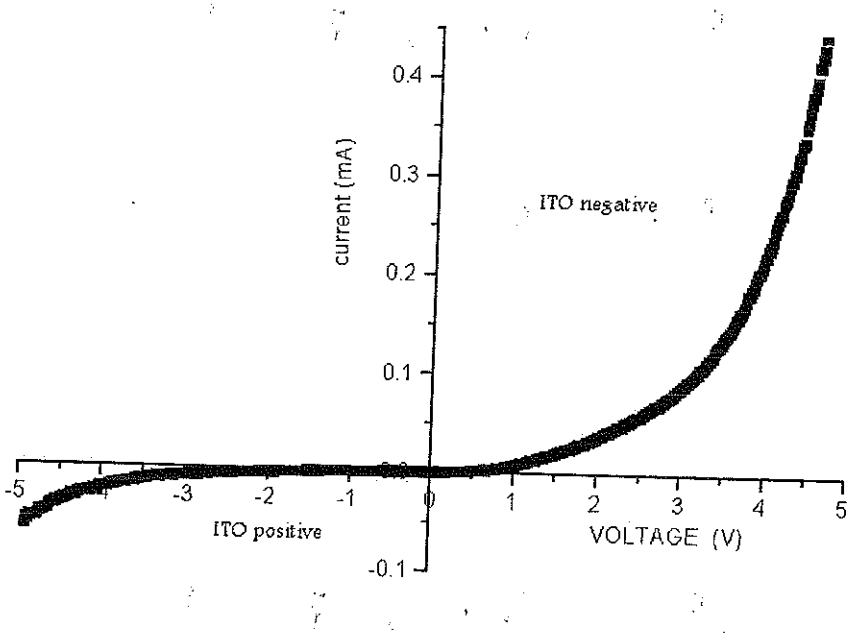

Figure 4.25. I-V characteristic curves for double layer arrangement ITO-poly (9-vinylcarbazole)-Rhodamine 6G-Al electrode.

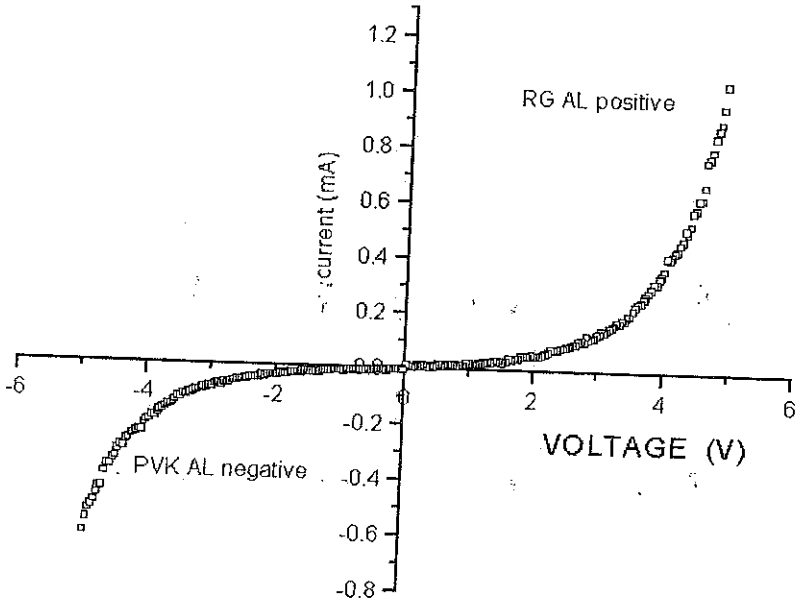

Figure 4.26. I-V characteristic curves for double layer arrangement Al-poly (9-vinylcarbazole)-Rhodamine 6G-Al electrode.

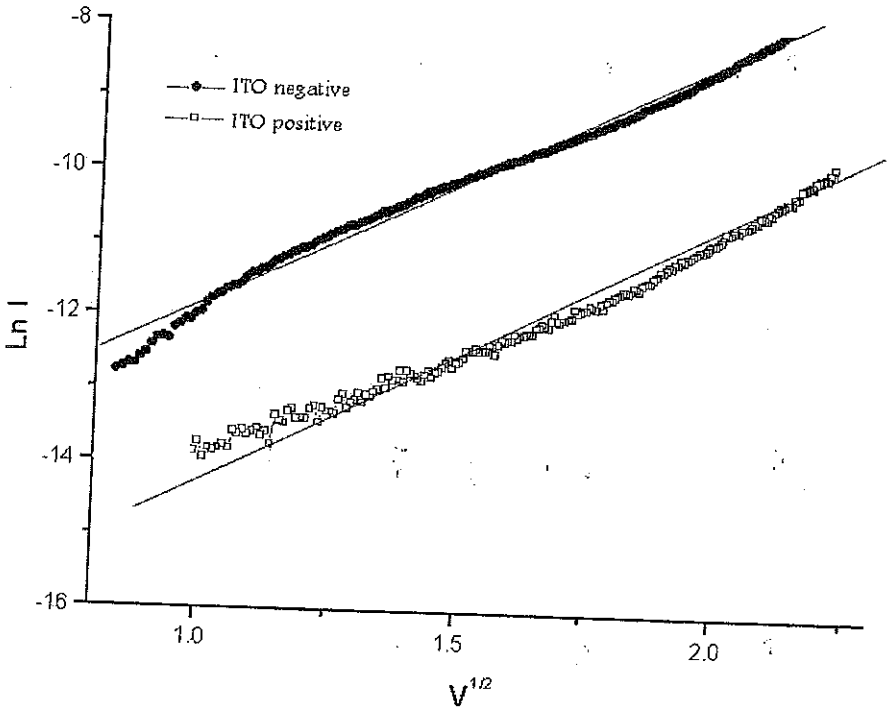

Figure 4.27. Plots of natural logarithm of the current versus square root of applied voltage for a double layer film arrangement ITO-poly (9-vinylcarbazole) –Rhodamine 6G-Al electrode.

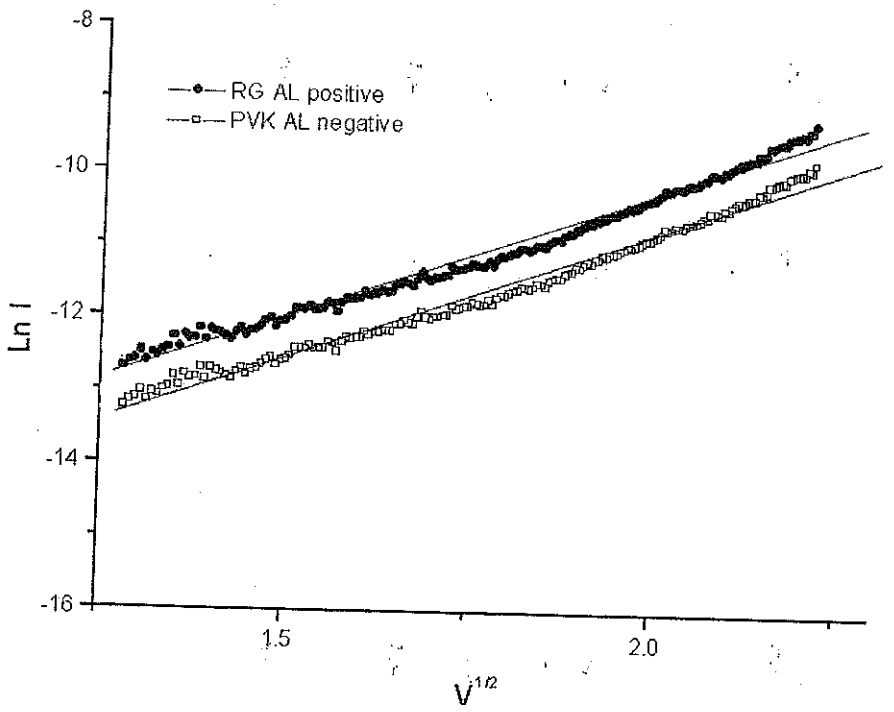

Figure 4.28. Plots of natural logarithm of the current versus square root of applied voltage for film double layer arrangement Al-poly(9-vinylcarbazole)-Rhodamine 6G-Al electrode.

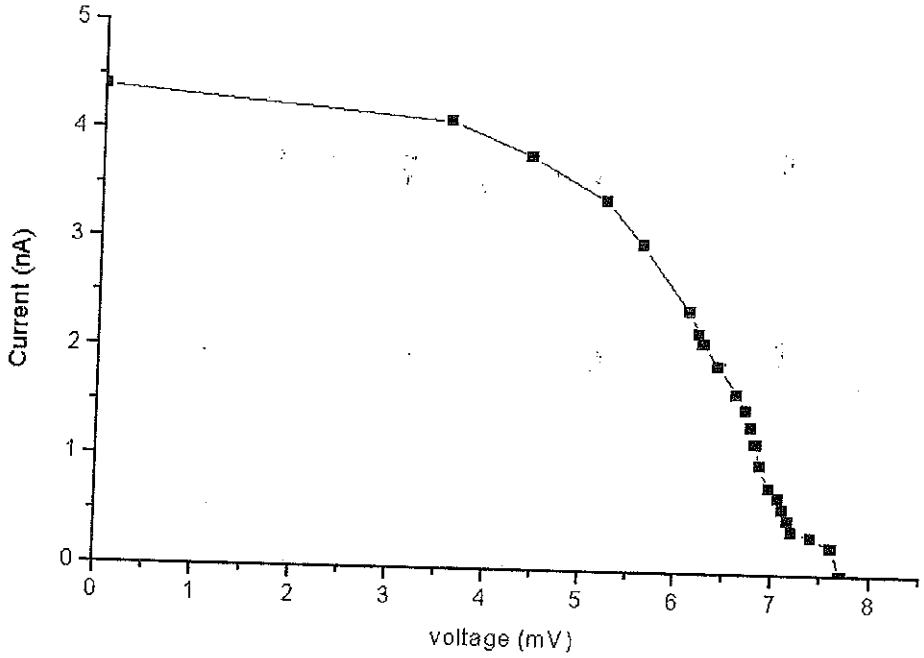

Figure 4.29. Plots of current versus voltage for film double layer arrangement ITO-poly (9-vinylcarbazole) doped with I_2-Rhodamine 6G-Al electrode.

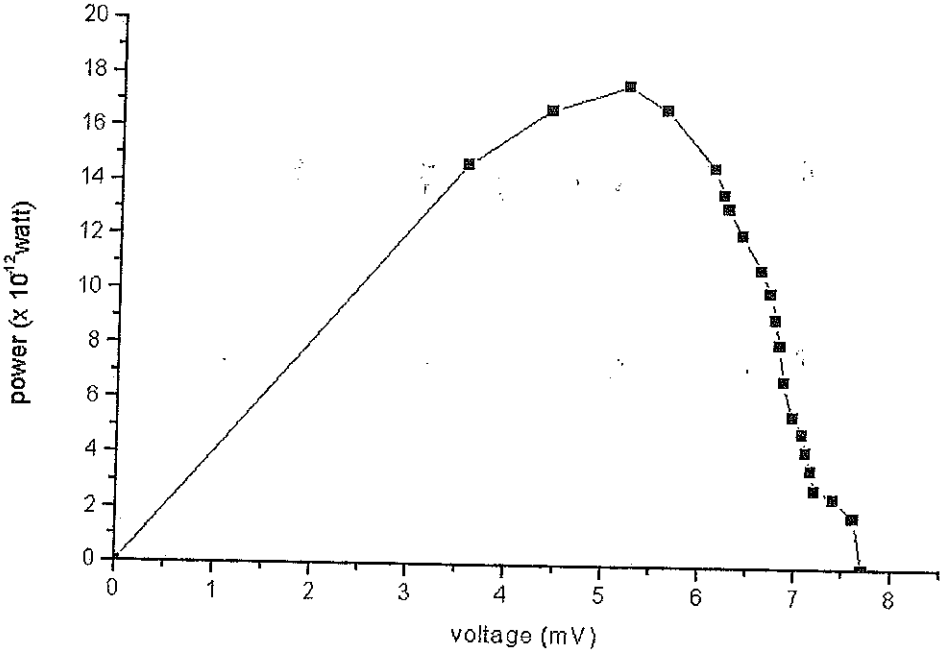

Figure 4.30. Plots of the power versus voltage for film double layer arrangement ITO-poly(9-vinylcarbazole) doped with I_2-Rhodamine 6G-Al electrode.

CONCLUSION

1340343

الجامعة الإسلامية - المكتبة - قسم الرسائل الجامعية

CONCLUSION

In this work, we conducted several measurements on single and double layer films with structure and composition as described in section 3.2. Among these measurements are the DC conductivity measurements, AC conductivity measurements, and photovoltaic effect measurements. All these measurements were done at normal atmosphere pressure. The DC conductivity I-V characteristic curves for Poly (9-vinylcarbazole) films doped with various concentrations of iodine have been studied. The current-electric field dependence in these films was found to obey the following relation,

$$I\alpha \exp\left(\frac{e\beta E^{1/2}}{kT}\right)$$

Also, the dependence of the current on the electric field for asymmetric electric electrodes structure was found to be dependent of polarities. This indicated that the conduction in these films obeys Schottky mechanism. Also, the double layer films obey Schottky mechanism.

It was found that the current in films doped with I_2 increases as the weight concentration of the dopant increases.

We found that the current flowing through a sample is dependent on the film thickness: the current flowing through thinner films is several times higher than the current flowing through thicker ones.

The thermal activation energy ε_a of the DC conductivity was studied at various dopant concentrations. We found that the values of ε_a are a typical of electron

conduction, which provide an evidence to our conclusion that the conduction mechanism is of an electronic type and obeys Schottky mechanism.

The *AC* conductivity for doped poly (9-vinylcarbazole) films with various weight concentrations have been studied as a function of frequency up to $3MHz$. At frequencies higher than $1KHz$ the *AC* conductivity increase almost linearly with frequency until about $0.5MHz$, then some kind of saturation is reached. On the other hand, the dielectric loss tangent was found to decrease with increasing frequency. Our data showed that the *AC* conductivity as a function of frequency has no dependence on film thickness and no role seemed to be played by the dopant molecule.

We found that the double layer samples (ITO-PVK doped with I_2-Al) exhibited weak photovoltaic effect with curve fitting factor c.f. equal to 0.54, short circuit current I_{sc} equal to 4.46 nA, and open circuit voltage V_{oc} equal to 7.7mV.

Finally, for farther development and improvement of this work we recommend the following:

1- Providing means for measuring the light intensity.

2- Providing means for performing the electrical and photovoltaic measurements under low pressure and low temperature.

3- Providing a technique for depositing samples with constant thickness in order to ease comparisons at different concentrations.

4- More work should be done to optimize parameters to obtain higher photovoltaic effect.

REFERENCES

REFERENCES

[1] Sarp Akcay, Arthur J. Epstein and Dr. Runguang Sun, Building Light Emitting Devices Based on Polymeric Substances, The Ohio State University, National Science Foundation, (2000).

[2] Mark E. Tuttle, Dept Mechanical Engineering, A brief Introduction to Polymeric Materials, University of Washington, Seattle, WA 98195-2600 (1999).

[3] A. Tager, **Physical Chemistry of Polymers,** Second edition, Translation from the russian by David Sobolev and Nicholas Bobrov, Mir publishers, (1978).

[4] R. j. young, **Introduction to Polymers**, First Edition, Chapman and Hall Pub. Co., New York, (1981).

[5] Ahmed. A. Eltayyan, A study of Electrical and Photoelectrical Conductivities of Poly(9-vinylcarbazole), Ph.D. Thesis, university of khartoum, khartoum, sudan, (1998).

[6] T. A. Geissman, **Principles of organic chemistry**, Second edition, McGraw-Hill, New York, (1977).

[7] P. Meares, **Polymers Structure and Bulk Properties**, First Edition, D. Van Nostrand Company Ltd. London, (1965).

[8] H. Warson, **Fundamentals of Polymer Chemistry**, Course Material Created, from http://media.wiley.com/product_data/excerpt/80/, (1965).

[9] F. W. Billmeyer, **Textbook of Polymer Science,** Second edition, Wiley-Interscience, New York, (1971).

[10] M. C. J. M. Vissenberg, Opto-Electronic Properties of Disordered Organic Semiconductors, Ph. D. Thesis, Proefcrift, Universiteit Leiden, (1999).

[11] W. Lenore Carman Rasmussen, Novel Carbazole Based Methacrylates, Acrylates, and Dimethacrylates to Produce High Refractive Index Polymers, Ph.D. Thesis, Blacksburg, Virginia Tech University, (2001).

[12] Encyclopedia Polymer Science and Engineering, edited by: H. F. Mark, John Wiley and Sons, Inc., New York, (1989).

[13] Shen Yue, Zhang Jiancheng, Gu Feng, Chen Jianming, Huang Haihua, Photoconductivity study of doping in C60-toluene derivative, Materials Chemistry and Physics, 72, 405–407, (2001).

[14] Alan J Heeger, Maria A Diaz-Garcia, Semiconducting polymers as materials for photonic devices,_Curr. Opinion. Solid St. Mtrls Sci., 3, 16-20, (1998).

[15] S. Touihri, P. Molinie, S. Ouro Djobo, K. Napo, G. Safoula, J.C. Bernede, Evolution with temperature of the ESR signal of bromine doped poly(N-vinylcarbazole) The doping temperature used as parameter, Polymer Degradation and Stability, 69, 333-340, (2000).

[16] S. C. Veenstra, Electronic Structure of Molecular Systems From Gas Phase to Thin Films to Devices, Pd.D. Thesis, University of Groningen, Netherlands, (2002).

[17] Klaus Petritsch, Organic Solar Cell Architectures, PhD Thesis, der Technischen University at Graz (Austria), (2000).

[18] J. Mort, G. Pfister, G. M. Sessler, Electronic Properties of Polymers, ED: J. Mort, G. Pfister, John Wiley and Sons, Inc., New York, (1982).

[19] R. Bahri, J. Phys. D, 15, 677 (1982).

[20] A. K. Sharma, V. Adinarayana and D. Santhi Sagar, Materials letters, 12, 247, (1991).

[21] M. Pfeiffer, A. Beyer, A. Nollau, T. Fritz, K. Leo, D. Schlettwein, S. Hiller, Controlled p-doping of pigment layers by cosublimation: Basic mechanisms and implications for their use in organic photovoltaic cells, Solar Energy Materials & Solar Cells 63, 83-99, (2000).

[22] H. Shirakawa, E. J. Louis, A. G. MacDiarmid, C. K. Chiang and A. J. Heeger, J. Chem. Soc.,Chem. Commun., 578, (1977).

[23] H. Naarmann and N. Theophilou, Synthetic Metals, 22, 1 (1987)

[24] J. Tsukamoto, Adv. Phys. 41, 509 (1992).

[25] Z. Bao, A. J. Lovinger, and J. Brown, New Air-Stable n-Channel Organic Thin Film Transistors, J. Am. Chem. Soc., 120, 207-208 (1998).

[26] David T. Wu, Theory for conductivity in conducting star polymer blends, Synthetic Metals 126, 289–293, (2002).

[27] Gouri S. Akundy, Ramakrishnan Rajagopalan, Jude O. Iroh, Electrochemical Deposition of Polyaniline–Polypyrrole, Composite Coatings on Aluminum, Materials Science and Engineering, University of Cincinnati, Cincinnati, Ohio 45221-0012, (2001).

[28] J. W. Gardner and P. N Bartlett, Applications of Conducting Polymer Technology in Microsystems, Sources and Actuators A 51, (1995).

[29] Furong Zhu, Keran Zhang, Ewald Guenther, Chua Soo Jin, Optimized indium tin oxide contact for organic light emitting diode applications, Thin Solid Films, 363, 314-317, (2000).

[30] B. Van Zeghbroeck, Principles of Semiconductor Devices, from http://ece-www.colorado.edu/ bart/book/, (2004).

[31] S. M. Sze, **Physics of Semiconductor Devices**, Second edition, John Wiley and Sons, Inc., New York, (1981).

[32] Jingshi Shi, Physics and Chemistry of Solid Interface, Institute for Micromanufacturing Louisiana Tech University, Ph. D. student of Engineering, (2002).

[33] J. Mort, G. Pfiste, G. M. Sessler, **Electronic properties of polymers**, John Wiley & Sons, Inc., NewYork, (1982).

[34] G. Safoula, K. Napo, J.C. Bern_ede, S. Touihri, K. Alimi, Electrical Conductivity of Halogen Doped Poly-(N-vinylcarbazole) Thin Flms, European Polymer Journal 37, 843-849, (2001).

[35] M. Allen, S. Diele, K. Harris, T. Hegmann, B. Kariuki, D. Lose, J. Preece, and C. Tschierskec, Intermolecular organisation of triphenylene-based discotic mesogens by interdigitation of alkyl chains, J. Mater. Chem., 11, 302-311, (2001).